Multiple domains of the integral KREPA3 protein are critical for the structure and precise functions of RNA editing catalytic complexes in *Trypanosoma brucei*

BRITTNEY DAVIDGE,[1] SUZANNE M. MCDERMOTT,[1,2] JASON CARNES,[1] ISAAC LEWIS,[1] MAXWELL TRACY,[1] and KENNETH D. STUART[1,2,3]

[1]Center for Global Infectious Disease Research (CGIDR), Seattle Children's Research Institute, Seattle, Washington 98109, USA
[2]Department of Pediatrics, University of Washington, Seattle, Washington 98195, USA
[3]Department of Global Health, University of Washington, Seattle, Washington 98195, USA

ABSTRACT

The gRNA directed U-insertion and deletion editing of mitochondrial mRNAs that is essential in different life-cycle stages for the protozoan parasite *Trypanosoma brucei* is performed by three similar multiprotein catalytic complexes (CCs) that contain the requisite enzymes. These CCs also contain a common set of eight proteins that have no apparent direct catalytic function, including six that have an OB-fold domain. We show here that one of these OB-fold proteins, KREPA3 (A3), has structural homology to other editing proteins, is essential for editing, and is multifunctional. We investigated A3 function by analyzing the effects of single amino acid loss of function mutations, most of which were identified by screening bloodstream form (BF) parasites for loss of growth following random mutagenesis. Mutations in the zinc fingers (ZFs), an intrinsically disordered region (IDR), and several within or near the carboxy-terminal OB-fold domain variably impacted CC structural integrity and editing. Some mutations resulted in almost complete loss of CCs and its proteins and editing, whereas others retained CCs but had aberrant editing. All but a mutation which is near the OB-fold affected growth and editing in BF but not procyclic form (PF) parasites. These data indicate that multiple positions within A3 have essential functions that contribute to the structural integrity of CCs, the precision of editing and the developmental differences in editing between BF and PF stages.

Keywords: *Trypanosoma brucei*; OB-fold; C2H2 zinc-finger; intrinsically disordered region; RNA editing

INTRODUCTION

Mitochondrial mRNAs in *Trypanosoma brucei*, the causal agent of Human African Trypanosomiasis (aka sleeping sickness), the related *T. cruzi* and *Leishmania spp*. pathogens, and other kinetoplastids undergo post-transcriptional maturation by RNA editing (Read et al. 2016). The editing generates mature functional mRNAs from transcripts by the insertion and deletion of U-nucleotides as specified by small guide RNAs (gRNAs) (Koslowsky et al. 1990; Pollard et al. 1990; Riley et al. 1994). Some mRNAs undergo quite limited editing, for example, the insertion of four or 34 Us in COII and CYb mRNAs, respectively, whereas editing essentially recodes the sequences of other mRNAs by extensive U-insertion/deletion for example, of +447/−28 and +547/−41 Us, respectively, in mRNAs for ATPase 6 and COIII oxidation-phosphorylation complex proteins and +132/−28 in RPS12 mitoribosomal protein mRNA (Benne et al. 1986; Feagin et al. 1987; Feagin et al. 1988; Bhat et al. 1990; Read et al. 1992). In addition, the editing of several transcripts differs between the life-cycle stages of *T. brucei* in parallel with its metabolic and developmental differences. Edited cytochrome subunit mRNAs are abundant in the insect midgut stage procyclic form (PF) parasites which generate energy via oxidative phosphorylation, whereas these edited mRNAs are dramatically reduced in the mammalian bloodstream form (BF) parasites that produce energy via glycolysis (Panigrahi et al. 2008). Thus, this differential editing adapts this pathogen to the disparate environments of the midgut of its tsetse fly vector versus the mammalian bloodstream (Feagin et al. 1987). The mechanisms responsible for this developmental difference

Corresponding author: ken.stuart@seattlechildrens.org
Article is online at http://www.rnajournal.org/cgi/doi/10.1261/rna.079691.123. Freely available online through the *RNA* Open Access option.

are unknown but do not appear to be due to differential gRNA abundances (Koslowsky et al. 1992; Riley et al. 1995).

RNA editing is catalyzed by three similar multiprotein catalytic complexes (CCs) that have different editing site (ES) specificities (Carnes et al. 2017). Each round of editing is initiated by cleavage of an ES by an endonuclease. Following cleavage, Us are either inserted by a terminal uridylyl transferase (TUTase) (Ernst et al. 2003; Deng et al. 2005) or removed by a U-specific 3′–5′ exonuclease (ExoUase) (Ernst et al. 2009; Carnes et al. 2012). Lastly, the ES is religated by an RNA ligase (McManus et al. 2001; Schnaufer et al. 2001; Stuart et al. 2002; Palazzo et al. 2003). Each CC contains a common set of 12 proteins including TUTase, ExoUase, and RNA ligase enzymes, as well as eight proteins (KREPB4, KREPB5, and KREPA1–6) that have no apparent catalytic function (Aphasizheva et al. 2020). Mutually exclusive pairs of endonucleases (KREN1–3 [N1–3]) and partner proteins (KREPB6–8 [B6–8]) functionally delineate each of the three CCs, one of which also contains an additional ExoUase (Schnaufer et al. 2003; Worthey et al. 2003; Carnes et al. 2017). KREPA3 (A3) is one of the noncatalytic proteins that is common to all three CCs. It contains two C2H2 zinc finger motifs (ZFs), a carboxy-terminal OB-fold motif, several intrinsically disordered regions (IDRs) but no other motifs that are related to known protein domains or predicted structures (Panigrahi et al. 2001; Schnaufer et al. 2010).

A3 is essential for cell growth and functions in RNA editing in both BF and PF life-cycle stages as has been shown by the loss of parasite viability and RNA editing upon A3 expression knockdown by RNAi or in conditional null (CN) cell lines (Guo et al. 2008, 2010; Law et al. 2008; McDermott et al. 2015b). Loss of A3 expression also affects CC structural integrity, albeit to a greater extent in BFs than in PFs, as shown by the retention of CCs in PF but not BF A3 CN cells (Brecht et al. 2005; Guo et al. 2008; McDermott et al. 2015b). Mutation analyses showed that the amino-terminal ZF (NTZF) and the more carboxy-terminal ZF (CTZF) domains are both required for parasite viability and RNA editing in BFs, whereas the latter ZF is not required in PF (Guo et al. 2008, 2010; McDermott et al. 2015b). Thus, the two A3 ZFs impact CC structure and function somewhat differently between these two life-cycle stages.

The carboxy-terminal region of A3 contains a prominent OB-fold domain with a β-barrel comprised of five strands (β_1–β_5). Like other OB-fold proteins, β_1 and β_2, β_2 and β_3, and β_4 and β_5 are connected by loops L_{12}, L_{23}, and L_{45}, respectively, while strands β_3 and β_4 are connected by an α-helix, C_{34} (Theobald et al. 2003; Horvath 2011). The region adjacent to the amino-terminal strand of the OB-fold is distinct from the corresponding region of the OB-folds of the other five CC proteins (A1,2, 4–6) (Park and Hol 2012). Previous studies have described the structure of the A3 OB-fold and its proximity to other proteins in the CC complex (Schnaufer et al. 2010; Park and Hol 2012; McDermott et al. 2016). Yeast two-hybrid and cross-linking-MS studies have shown that the A3 OB-fold interacts with KREPB5 (B5), another noncatalytic CC protein and is proximal to several other proteins in CCs, including the N1 deletion endonuclease (Schnaufer et al. 2010; McDermott et al. 2016), N2 insertion endonuclease and the five other OB-fold containing proteins (Schnaufer et al. 2010; McDermott et al. 2016). Previous studies have shown that the OB-fold can interact with RNA in vitro and has RNA chaperone activity (Brecht et al. 2005; Voigt et al. 2018). Structure determination of recombinant A3 and A6 co-crystals identified interactions between A3 and A6 OB-folds within the crystal lattice (Park and Hol 2012; Park et al. 2012b). Thus, the A3 OB-fold likely plays a structural role in CCs via its interactions with other CC proteins, including close interactions with A1–A6 as shown by cross-linking studies (Schnaufer et al. 2010; McDermott et al. 2016; Voigt et al. 2018). However, the specific functional roles of A3 in vivo in CC structure and editing and how they may differ between BF and PF stages are unknown (Schnaufer et al. 2002; McDermott et al. 2015b).

We report here the identification of multiple single amino acid (saa) mutations that result in loss of function (LOF) in BFs and in one case in PFs. Most of these substitutions mapped to the two ZFs, an IDR in a region with no predicted structure, or adjacent to the OB-fold. Exclusive expression of some of these mutant alleles resulted in loss of all three CCs and editing in BFs but not in PFs, except in one case where CCs and editing were reduced but not eliminated in PFs. Other mutations had lesser effects on CC structure and altered but did not eliminate RNA editing, and some of these mutations had differential effects on CCs and editing that were generally more impactful in BFs than in PFs. These results indicate that A3 interacts with multiple proteins in the three CCs and contributes to their structural organization and integrity, and that various A3 domains identified by these mutations have specific functions among the numerous events that occur during editing. These functions likely occur via specific molecular interactions that may differ among the three CCs which possess different ES specificities. The differential effects of the mutations between BF and PF cells imply that some of these A3 domains function differently between these stages despite the indistinguishable protein compositions of CCs (Carnes et al. 2011).

RESULTS

Mutations that affect growth of BFs are in multiple protein domains

To elucidate the role of A3 in editing, we tested 634 BF CN cell lines that had been cloned in wells by dilution after transfection with a library that contained ~10,000 unique full length randomly mutated *A3* alleles. We identified

136 wells with growth defects by replica plating in the presence or absence of tet as previously described (Supplemental Table S1; McDermott et al. 2015a). PCR and sequencing of *A3* from 59 wells that had strong growth defects identified 14 mutations of interest from sequences that (i) had a single amino acid substitution, the same substitution in multiple clones that had multiple mutations, or a substitution that likely would have a functional consequence based on structural analyses, and (ii) which reproduced the growth defect upon exclusive expression in cells in which the mutation was independently reconstructed by site-directed mutagenesis (Fig. 1A; Supplemental Fig. S1). Three single substitutions (Q299H, L262P, and T315A) did not reproduce the growth defects upon reconstruction and thus these residues are not critical for A3 function in BFs. These may have either originated from wells in which the screened cells were not clonal (Q299H) or not be the mutation responsible for the growth defect in clones with multiple substitutions (L262P and T315A). The number (14) of confirmed single amino acid substitutions that affect A3 function is similar to that identified in B5 (9), B6 (12), B7 (10), and B8 (9) by similar methods (McDermott et al. 2015a; Carnes et al. 2022). We also constructed cell lines with double amino acid substitutions in the more amino- and carboxy-terminal ZFs (NTZF and CTZF) with an amino-terminal V5 tag for comparison with previous constructs carrying the same mutations but with different epitope tags (Supplemental Table S2; Guo et al. 2008, 2010).

The confirmed LOF mutations localized to the two ZF domains and to various positions near or within the OB-fold (Fig. 1A). They were mapped to the partial A3 structure that had been determined by X-ray crystallography and a

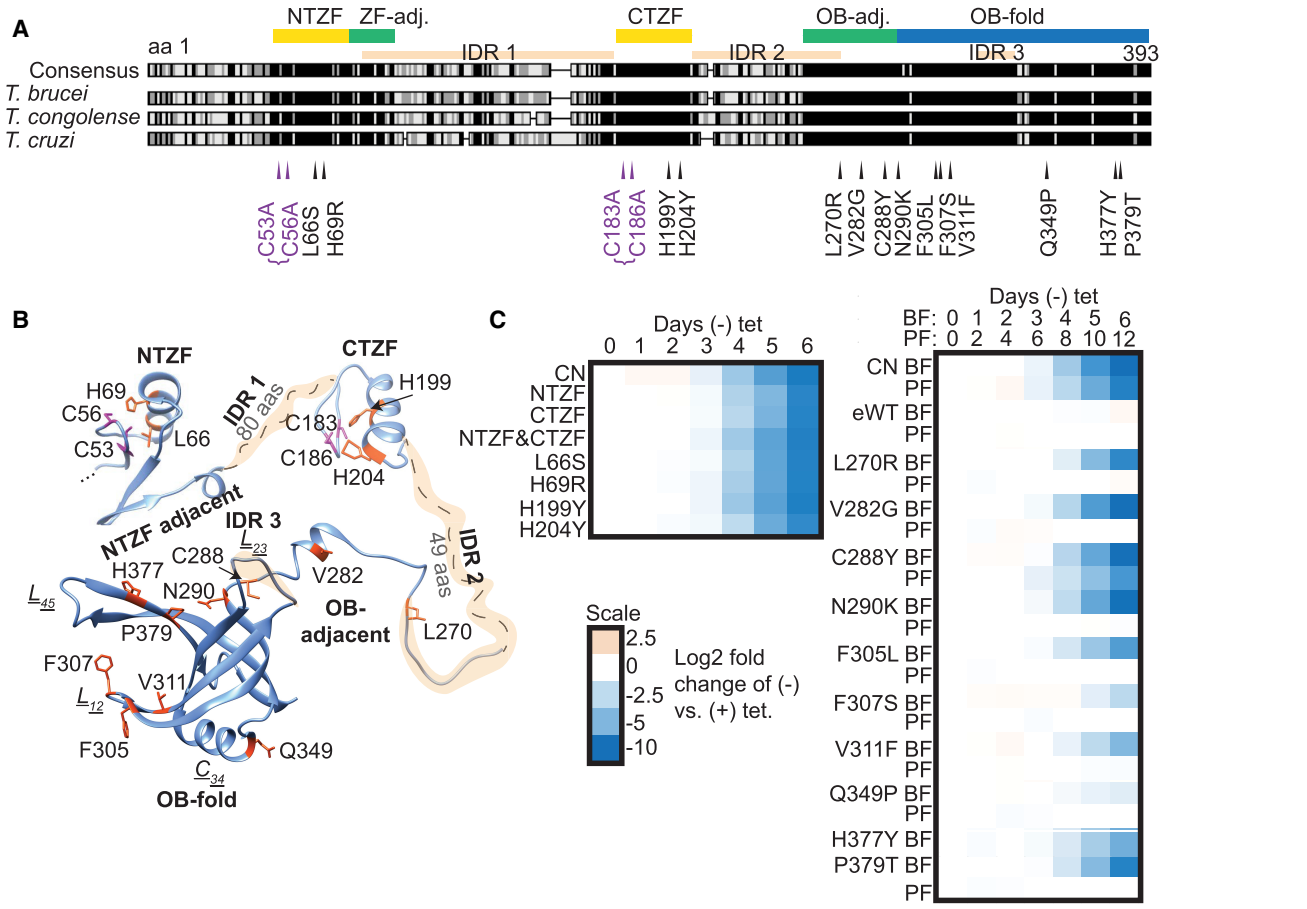

FIGURE 1. Loss of function mutations in A3 and their effects on growth. (*A*) Locations of single and double (bracketed) amino acid substitutions that resulted in loss of growth in BF *T. brucei* when exclusively expressed. Substitutions are mapped against a sequence alignment of three Trypanosoma species. Sequences were obtained from TriTrypDB and analyzed using Geneious (see Materials and Methods for gene IDs). MUSCLE alignment was highlighted using the Blosum 62 matrix, threshold 1. Black indicates amino acid similarity in all three species, and gray indicates similarity in two out of the three. The locations of the NTZF and CTZF (yellow); the OB-fold (blue) and the regions adjacent to these (green) are indicated as are three IDRs (tan). (*B*) Location of the substitutions in a composite A3 structure of a high confidence AlphaFold structural prediction (veb8-A) and crystal structure of the OB-fold (PDBID: 4DNI, Park and Hol 2012). Single amino acid substitutions are in orange and double C → A substitutions are in magenta. (*C*) Effect on growth after A3 repression (CN) or of exclusive expression of A3 (i.e., −tet) with substitutions in or near the ZFs (*left*) or in or near the OB-fold (*right*) over 6 d in BFs and 12 d PFs (see Materials and Methods for details). "eWT" indicates exclusive expression of the *V5-WT* allele from the *tubulin* locus under −tet conditions. Heat maps shown represent one biological replicate.

full-length A3 structure that was predicted using AlphaFold (Fig. 1B; Park and Hol 2012; Jumper et al. 2021). The double mutations in the ZFs map to regions that are adjacent to a helix that is in each ZF, the single substitutions map to similar positions within these small helices in each ZF, which except for L66S are likely to impact coordination of one or both Zn^{2+} ions coordinated by C2H2 ZF domains similar to the two double mutations. The region adjacent to the NTZF has predicted β-strands that contain many charged lysine and glutamate residues. The features of these ZF domains imply that they participate in RNA and/or protein interactions. The other single mutations mapped to a region adjacent to the amino-terminal side of the OB-fold which includes one of the predicted IDR inter-domains and a small helical region and to multiple positions within the highly structured OB-fold (Fig. 1B). The single and double mutations in the ZFs had substantial impacts on growth of the BFs (Fig. 1C); the single ZF mutations were not tested in PFs, but double mutations in the NTZF but not the CTZF substantially inhibit growth in PFs (McDermott et al. 2015b). The mutations that mapped to the region that is adjacent to or in the first strand of the OB-fold (V282G, C288Y, and N290K) or the nearby disordered region (L270R) that was previously predicted (Park and Hol 2012) also had substantial impacts on growth (Fig. 1C). The mutations that mapped to the core of the OB-fold β-barrel structure or in or near loops L_{12} and L_{45} (F305L, F307S, V311F, Q349P, H377Y, and P379T) had lesser effects on growth. All mutations throughout the OB-fold and the nearby region, except C288Y and C53A/C56A mutations in the NTZF, resulted in growth defects in BFs but not in PFs, indicating that these domains may function in the differential editing that occurs between these life-cycle stages (Fig. 1C; McDermott et al. 2015b).

Mutations of A3 affect CC abundance and integrity

Blue Native (BN) or SDS-PAGE and western analysis of lysates from the reconstructed A3 mutant BF and PF cell lines with LOF mutations of A3 revealed various effects on CC structural integrity and abundance of CCs and their proteins (Fig. 2). The ∼1 MDa complexes, four CC proteins and tagged A3 protein were evident in cells that exclusively express WT A3 (eWT) from the *tubulin* locus using mAbs for A1, A2, A3, and KREL1 (L1) CC proteins, the V5 tag on A3 and mt HSP70 that was used as a loading control. The parental CN cells, which do not have the tagged *A3* allele, lacked CCs and the four CC proteins when A3 expression from the *rDNA* locus was repressed (−tet). This shows both the stringent loss of A3 protein during exclusive expression, that is, −tet, and that A3 is required for the presence of CCs and these CC proteins. A3 consistently runs with a slightly smaller apparent size in the L270R mutant in both BF and PF cells. Genomic DNA sequencing confirmed that the *L270R* allele is full length, indicating that the mutation itself alters its apparent size, perhaps due to an added charge from Arg. Conversely, A3 has a slightly larger apparent size in CTZF single H199Y and H204Y and double C183A/C186A mutants in BFs, perhaps due to disruption of Zn^{2+} ion coordination. We cannot exclude the possibility that these differences may be due to other processes such as post-translational modifications (PTMs). V5-tagged A3 mutants were present in similar cellular amounts, except in C288Y in which there was CC loss. The A3 mutant proteins detected with the V5 mAb were ∼50 kDa in size, as expected, whereas the mutants detected with the A3 mAb were ∼42 kDa in size. This size difference is consistent with the amino-terminal V5 tag being cleaved off upon import into the mitochondrion, which would be consistent with an unidentified mitochondrial targeting sequence (MTS) cleavage site within A3. A3 detected with the A3 mAb appeared more variable in amount which correlated with the abundance of CCs and the other three CC proteins.

The abundance and integrity of CCs and the four CC proteins (A1, A2, A3, and L1) differed between the various mutant cell lines (Fig. 2). The ∼1 MDa CCs and the four CC proteins are abundant in all BF cell lines containing mutations in the ZFs, but a smear below the ∼1 MDa band suggests some impact on CC structural integrity, which is more apparent with mutations in the NTZF with parallel effects on the levels of the four CC proteins assayed. Mutations that are in or near the OB-fold had various effects on the CCs and their proteins (Fig. 2). The V282G, C288Y, and N290K mutants, and to a lesser extent the F305L mutant, had lost most of the ∼1 MDa CCs and the four CC proteins. There were somewhat lower CC and protein losses in the F307S and P379T mutants. However, these mutants also contained an ∼800 kDa complex that was also prevalent in V311F and P379T mutants, reminiscent of previously observed subcomplexes (Carnes et al. 2022). There was a general correlation between CC abundance and severity of growth defect for BF cell lines with mutations in or near the OB-fold, as cell lines with fewer intact CCs had greater growth defects (Figs. 1, 2). This was not the case for the ZF or disordered region (L270R) mutants, which have abundant ∼1 MDa CCs but substantial growth defects (Figs. 1, 2).

Together, these data suggest that although the ZFs are important for CC integrity in BFs, they likely play additional functional roles, for example, RNA binding that contributes to the substantial growth defects associated with their mutation. Mutations in or near the OB-fold were also tested in PFs, for which only C288Y has any notable impact on the CCs (Fig. 2). In these cells, a smeared band can be observed on the BN-PAGE gel with sizes ranging from ∼800 kDa to 1 MDa, indicating CC fragmentation (Fig. 2). V282G and N290K, which have normal growth in PFs, have CCs that might also be fragmented, although the extent of fragmentation is less than in C288Y (Fig. 2). Previous studies have shown that the CTZF is not necessary for growth or CC integrity in PFs, but the NTZF is required for PF growth

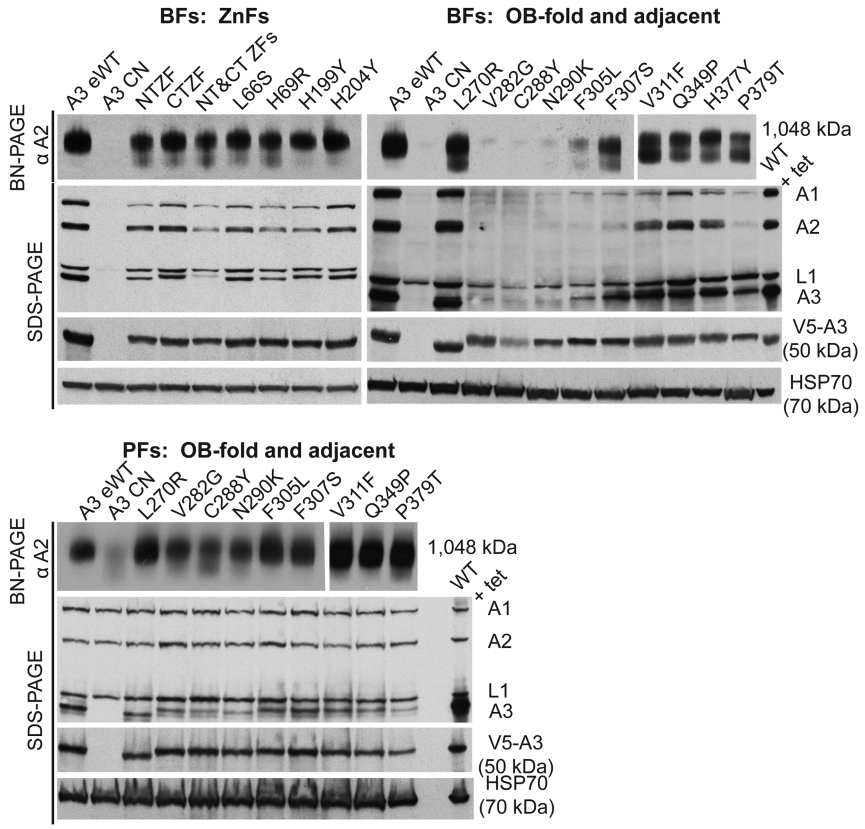

FIGURE 2. Effects of A3 mutations on catalytic complexes. Western analyses of blots analyzing cleared cell lysates after either 48 h (BF) or 96 h (PF) of exclusive expression of either mutated, wild-type, or no A3 (CN) using BN-PAGE (*upper* panel) and denaturing PAGE (*lower* panels). The BN-PAGE blots were probed with a mAb for A2 which is present in all CCs; the denaturing PAGE blots were probed with a mAb mixture for four CC proteins or mAbs for the V5 tag on A3, or the HSP70 loading control. Note the greater effect on the CCs in BF (*upper*) versus the PF (*lower*). Western blots shown represent at least two biological replicates.

(McDermott et al. 2015b). Together, these results suggest that different parts of A3, including the OB-fold, disordered region, and at least one ZF, contribute differently to CC structure between life-cycle stages.

The effects on CCs which were retained in the BF L66S, L270R, V311F, H377Y, and P379T mutants were examined in more detail by glycerol gradient fractionation. Fractions were analyzed by BN-PAGE and SDS-PAGE followed by western blotting (Fig. 3). The CCs from eWT, L66S, L270R, and H377Y sedimented with a peak at ~20S (fractions 13–17) as detected by mAbs for four CC proteins (Fig. 3A,B). The blots were also probed with a mAb for RESC1, a component of the RNA editing substrate complex (SC) with which CCs functionally interact (Aphasizheva et al. 2014), and with a mAb for HSP70 as a loading control (Fig. 3B). The mutations resulted in various reductions in the amounts of CCs per cell, as shown by western analyses of lysates prepared using equivalent cell numbers. Mutations in the NTZF (L66S) and the IDR (L270R) cause minimal, if any, loss of CCs, whereas mutations in strands β5 (H377Y and P379T) and β2 (V311F) of the OB-fold had greater CC loss but all retained some ~20S CCs. The V311F and P379T mutants had visible ~800 kDa bands in fractions 9–11 in the BN-PAGE westerns and preferential loss of the A1 CC protein in the SDS-PAGE blots. In addition, the bulk of the complexes in these mutants are shifted to lower S value regions of the gradient where the preferential loss of A1 and A2 is evident in the direct comparisons (Fig. 3C). These results are consistent with the loss of the ~186 kDa A1-containing heterotrimeric insertion subcomplex and retention of an ~800 kDa subcomplex comprised of the L1-containing heterotrimeric deletion subcomplex and other CC proteins (Carnes et al. 2022). The detection of A3 at low S value regions of the gradient with anti-V5 antibody but not anti-A3 antibody likely is due to a combination of the effects of the greater sensitivity of the V5 antibody and of the amino-terminal V5 tag which may have affected incorporation into CCs, and/or MTS processing and transit into the mitochondrion. Some tagged A3 might also be unincorporated due to its possible relative overexpression. The mutations had no appreciable effect on the abundance or distribution of the RESC1 component that binds gRNAs (Weng et al. 2008; Hashimi et al. 2009; Aphasizheva et al. 2020) and functionally interacts with CCs (Aphasizheva et al. 2020). Overall, these results illustrate the role of A3 in the structural organization of CCs, and the disruption caused by the V311F mutation signifies the importance of a hydrophobic pocket in A3 that includes V311 (Park and Hol 2012) for CC structural integrity.

Effects of A3 mutations on RNA editing

The effects of selected BF and PF A3 mutations on RNA editing in vivo were assessed by high-throughput RT-qPCR using the Fluidigm BioMark system (McDermott et al. 2015b). The abundances of amplicons from pre-edited, edited, and never-edited mitochondrial mRNAs in BF and PF cells that were exclusively expressing WT or mutant *A3* alleles were assayed prior to the effect on cell growth relative to those in the corresponding cells in which the tet-regulatable *WT A3* allele was expressed (Fig. 4A; Supplemental Table S2). The abundances of most edited

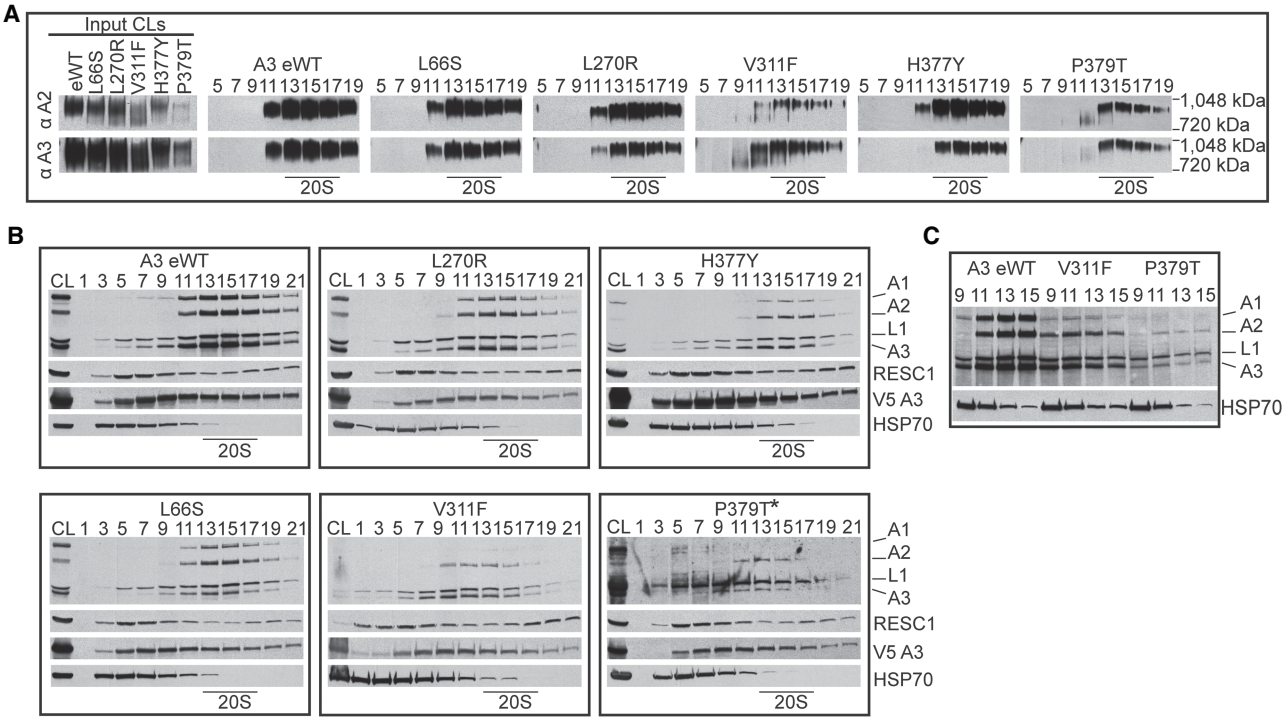

FIGURE 3. Glycerol gradient analysis of the effects of A3 mutations on catalytic complexes. Western analysis of 10%–30% glycerol gradient fractions from lysates of the indicated cell lines probed with indicated mAbs as in Figure 2. The gradients shown represent two biological replicates for eWT and P379T and one biological replicate for L270R, L66S, V311F, and H377Y. (*A*) Blots of BN-PAGE of input cleared lysates (CLs) and gradient fractions. (*B*) SDS-PAGE followed by western blotting of input CL and of glycerol gradient fractions probed as in *A*. The P379T* blot used super-signal ECL and was exposed longer. (*C*) Selected gradient fractions for direct comparisons among eWT, V311F, and P379T.

transcripts were reduced upon exclusive expression of mutant relative to WT A3 in BFs. The lack of detectable edited CYb mRNA in BFs or 3′ domain edited ND7 mRNA in PFs reflects their known developmental regulation (Schnaufer et al. 2002; McDermott et al. 2015a). The reductions in edited transcript levels in BF mutant samples generally correlated with the severity of growth defect and CC abundance, for example, V282G, C288Y, or N290K mutations had the greatest decreases in editing. An exception to this is that the L270R mutation did not impact CC abundance in BFs but had a substantial reduction in edited mRNAs and a moderate growth defect (Fig. 4 compared with Figs. 1 and 2). Strikingly, the effects of these mutations on the abundances of the edited PCR products differed between BF and PF life-cycle stages and mirrored the impacts on growth and CC abundance. Only one OB-fold mutation (C288Y) impacted edited mRNA levels in PFs, which is consistent with the growth defect caused by this substitution in PFs (Fig. 4A). Thus, A3 functions differently in editing between the life-cycle stages.

These qPCR analyses provide an overview of targeted pre-edited and edited mRNA amplicon abundances but do not measure partial or anomalous editing resulting from the mutations. We therefore generated profiles of all these RNAs from BF and PF cells by performing RT-PCR using primers that anneal to the mRNA 5′ and 3′ terminal regions of the mRNAs that do not get edited, resulting in amplification of all products regardless of how much editing occurred. We analyzed ATPase 6 (A6), RPS12, and MURF2 mRNAs which are edited in both life-cycle stages and used never-edited ND4 mRNA as a control (Fig. 4B). We resolved the resultant products on an agarose gel to visualize the editing products associated with each exclusive expression cell line (Fig. 4B). Because edited mRNAs contain more insertion sites than deletion sites, larger products result from more editing, and thus more editing occurred in cell lines with larger products. The A3 CN cell line in both the presence and absence of tet was included as a control. The different mutations resulted in distinct RT-PCR product profiles (Fig. 4B). In BFs, the single L66S, H69R, H199Y, and H204Y mutations in the helical regions of either ZF and the double C183A/C186A mutation in the CTZF resulted in A6 profiles that were distinct from the conditional null in the presence or absence of tet, which suggests that some editing occurred but was likely anomalous or incomplete, similar to what has been previously described for double mutation in the ZFs (Guo et al. 2010). A similar result was observed for RPS12 except the single mutants had more pre-edited size product in comparison to the CN +tet. The double C53A/C56A mutation

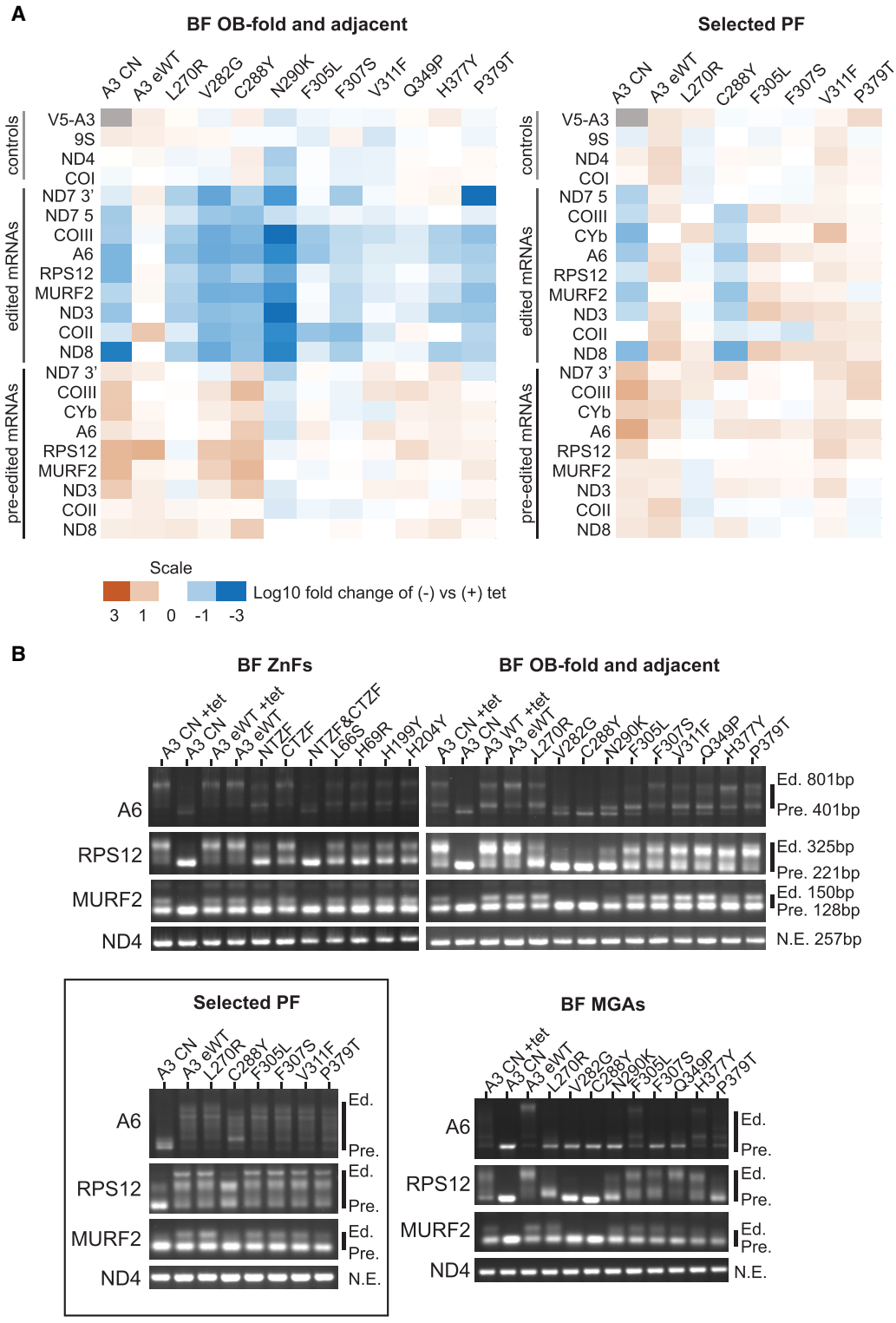

FIGURE 4. Impacts of A3 mutations on RNA editing. (*A*) qPCR measurements of pre-edited and edited mRNAs as indicted in samples from BF and PF cells grown in the presence or absence of tet for 48 and 96 h, respectively. The levels of RNAs were normalized to the TERT control. Relative abundances of mRNAs (−tet vs. +tet) were then determined for each sample, transformed by $\log_{10}$, and represented by a heat map. The measurements are representative of up to three biological replicates with two technical replicates for each; see Materials and Methods for details. (*B*) Gel profiles of RT-PCR products with pre-edited (Pre) and fully edited (Ed.) sizes as indicted are from cells grown for 48 h (BF) or 96 h (BF with an *MGA* allele or PF) following tet removal. Only minus tet samples are shown unless indicated otherwise. (Box) Selected PF cell lines that represent different regions of the OB-fold; most mutations do not result in growth defects in PF. The profiles shown represent two biological replicates for the CN-background cell lines and one replicate for the MGA cell lines.

of the NTZF alone or together with the double mutation of the CTZF resulted in greater amounts of pre-edited sized product, which is indicative of reduced editing. These results and those with the double mutation in the NTZF and/or CTZF in BF and PF CN cells that exclusively express a carboxy-terminal TAP-tagged (BF) or untagged (PF) A3 reinforce the role for the A3 ZFs in editing (Guo et al. 2008, 2010; McDermott et al. 2015b).

Mutations in or near the OB-fold had more variable effects on editing which were parallel to their effects on CC structure. The V282G, C288Y, and N290K substitutions which resulted in substantial loss of CCs and their proteins (Fig. 2) had predominant RT-PCR products consistent with pre-edited mRNAs or short partially edited products (Fig. 4B). The F305L mutant that had reduced, but not eliminated CC abundance had larger RT-PCR products consistent with partially edited sizes. Similar partially edited products were also observed with F307S, V311F, Q349P, H377Y, and P379T mutants that broadly retained CC proteins. Interestingly, the L270R mutant that retained CCs had a similar A6 RT-PCR profile to that of these five other mutants but had a unique, prominent RPS12 product that was slightly larger than the pre-edited size (Fig. 4B).

Analysis of the effects of a subset of the OB-fold mutations on editing in PFs by gel analysis of the RT-PCR products of the A6, RPS12, and MURF2 mRNA showed more products that are larger than pre-edited than in BFs which reflect the presence of CCs in PFs. The sizes of the RNAs are similar to those in the eWT with the exception of the C288Y mutants where smaller products are seen (Fig. 4B). Thus, mutations in the OB-fold that were assayed in PFs resulted in different effects on editing than in BFs and indicated functional differences of the A3 OB-fold between these developmental stages.

We transfected a *mutant gamma ATP synthase (MGA)* allele into the BF A3 CN cell line and then reproduced some of the mutant cell lines and eWT to enable the survival and continuous growth of BFs in the absence of RNA editing (Fig. 4B; Supplemental Fig. S2; Dean et al. 2013; Carnes et al. 2017, 2023). This allowed us to assess possible incomplete development of the effects of the mutations or secondary effects of the mutations, for example, physiological consequences due to loss of products encoded by edited mRNAs. Because the MGA cells can survive without RNA editing, we were able to assess editing in these cell lines 96 h after tet removal instead of the 48 h used for the CN cells. This resulted in a shift to a greater proportion of products with sizes at or near that of pre-edited mRNA (Fig. 4B). This was especially evident for the V282G and C288Y mutations that lack most CC material (Fig. 2; Supplemental Fig. S2) and with the longer A6 and RPS12 mRNAs. The other mutations had products that were larger than pre-edited but generally smaller than the largest product in wild-type. The L270R mutant retained ample ~1 MDa CCs but the RT-PCR product appeared slightly longer than pre-edited (Fig. 2). Overall, these results suggest that editing occurred in mutants that retained CCs albeit insufficient in amount or accuracy to support growth.

To determine the characteristics of the RT-PCR products, we sequenced multiple RPS12 PCR products that range in size from ~221 bp (pre-edited) to 325 bp (fully edited) that we cloned from cell lines that retained various proportions of ~1 MDa and ~800 kDa CCs following 48 h of growth in the absence of tet. As shown in the diagram (Fig. 5), these sequences indicated that editing had occurred in all four cell lines, although it was incomplete compared to fully edited RNA. However, a two-tailed *t*-test indicates that in the L270R mutant the extent of editing (defined as number of sites with any editing, that is, the number of Us do not match pre-edited RPS12) is significantly less compared to WT (Fig. 5; Supplemental Fig. S3; Supplemental Table S3). Additionally, the proportion of fully edited insertion ESs were reduced and the proportions of deletion ESs that were not fully edited and of editing in nonedited ESs were increased, an effect that seemed to manifest near ES 25, which is within the region spanned by either gRPS12 (288–302) or gRPS12 (269–308) (Fig. 5; Supplemental Fig. S3; Kirby et al. 2016). A previous study of RPS12 sequences from cell lines with components of the RNA-binding SC knocked down observed altered editing in this region of the transcript; however, the sequences we show here differ from those in the other study (Dubey et al. 2021). In the F307S and P379T mutants the extent of editing was greater than in L270R, and not statistically different than the WT (Supplemental Fig. S3; Supplemental Table S3). These results show that these mutants perform editing but do so with reduced accuracy and/or efficiency that is insufficient for cell viability.

Structural comparisons and functional context of the effects of A3 mutations

A Dali search (Holm 2022) for *T. brucei* structural homologs of A3 identified the A1, A2, and A4–6 OB-fold containing CC proteins as expected (*z*-scores of 14.7, 12.6, 10.6, 13.7, 13.4, respectively). It also identified Tb927.9.4810 MPSS5 (*z*-score 10.0) and Tb927.6.2190 MPSS6 (*z*-score 11.1) components of the MPsome complex that has TUTase and exonuclease activities and gRNA processing functions (Aphasizheva et al. 2020), and Tb927.10.8220 (*z*-score 11.1) an uncharacterized protein that has been observed in isolations via KRET1, DSS1, and MPSS2 pull-downs and whose gene is adjacent to A2 (Fig. 6A; Penschow et al. 2004; Aphasizheva and Aphasizhev 2016; Suematsu et al. 2016; Aphasizheva et al. 2020). All these proteins have predicted OB-folds similar to A3, with amino acids that align with those identified as critical for A3 function (Supplemental Tables S4, S5; Supplemental Fig. S4). Additionally, MPSS5 has a C2H2 ZF similar to A3, while MPSS5 and MPSS6 have predicted helical domains and regions with no predicted structures that may contain IDRs, all features

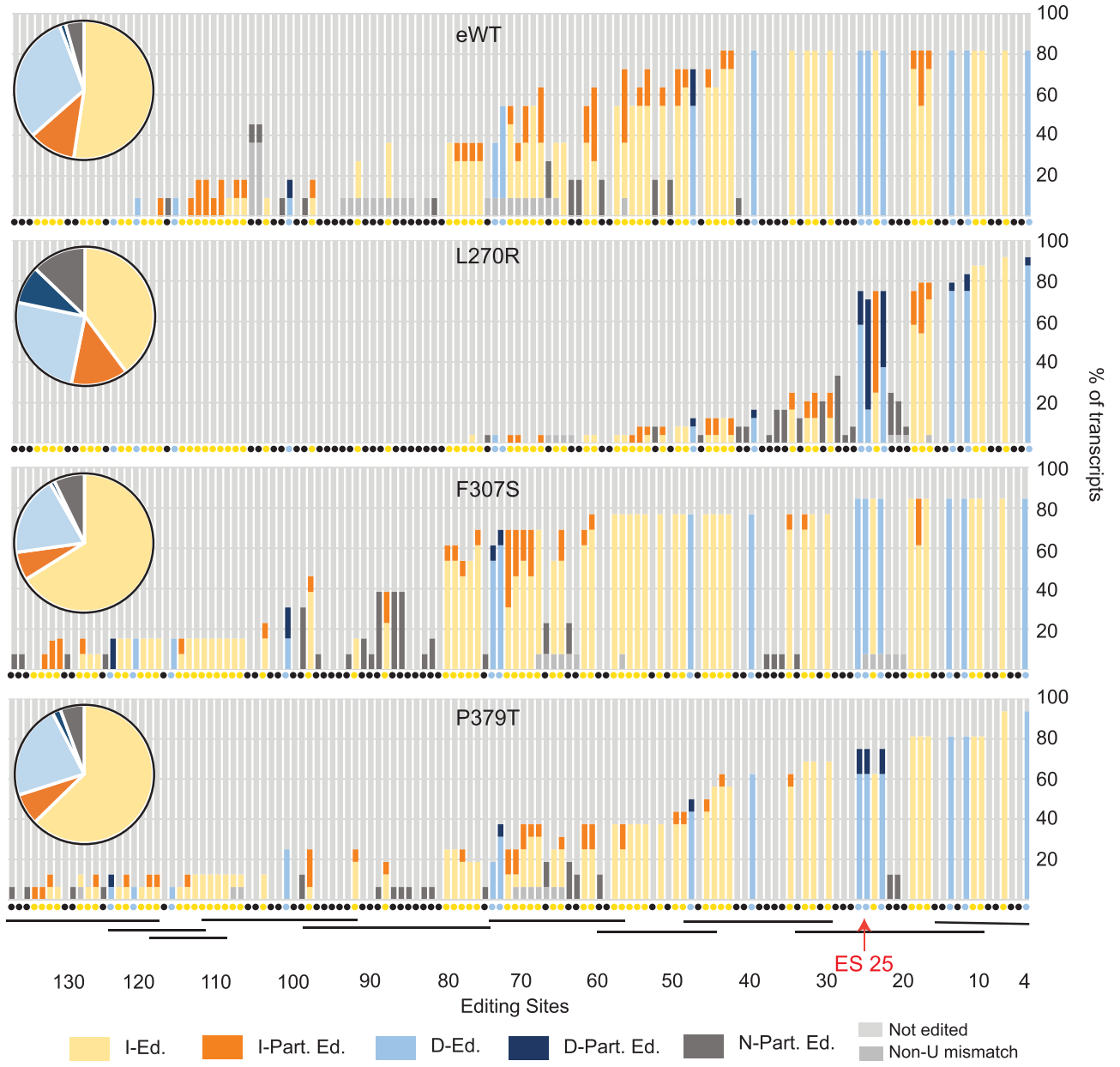

FIGURE 5. Impacts of A3 mutations in BF cell lines on cloned RPS12 sequences. A summary of the editing of cloned and sequenced RPS12 mRNAs (Supplemental Fig. S3) is summarized by the bar graph that shows the percent of the type of editing at each ES classified as (I-Ed.) fully edited insertion ES (yellow), (I-Part. Ed.) partially edited insertion ES (orange), (D-Ed.) fully edited deletion ES (light blue), (D-Part. Ed.) partially edited deletion ES (dark blue), (N-Part. Ed.) partially edited ES that is not edited in fully edited mRNA (dark gray). ESs where no editing was observed (light gray) and ESs impacted by a non-U mismatch (medium gray) are shown. Each type of editing event is shown as a percent of the total for each sample in the pie chart inserts. The colors of the small circles *beneath* each bar indicate the type of editing at each ES in fully edited mRNA. The approximate locations of gRNAs that can specify the edited sequences are shown by black bars (Kirby et al. 2016) and ES 25 is indicated.

that imply functional interactions with RNA and/or protein (Fig. 6A). In the structural overlays, a Val is present in eight of the nine OB-folds at the position that is equivalent to V311 in A3, and a Pro is present in seven out of the nine at the position that is equivalent to P379 indicating their functional importance in these OB-folds (Supplemental Table S5; Supplemental Fig. S4). A summary of findings showing relationships between CC structure and RNA editing is shown in Figure 7.

DISCUSSION

We show here that multiple functional domains of A3 are essential for structural integrity and accurate functioning of the

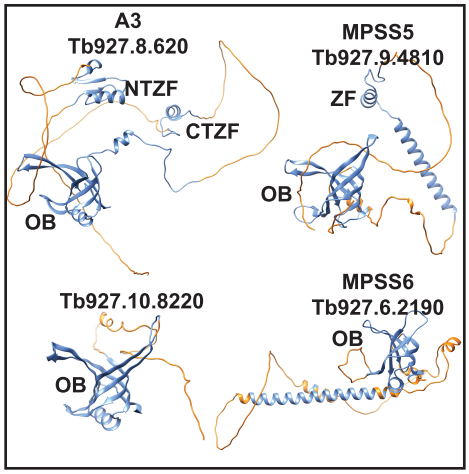

FIGURE 6. Structural similarities between A3 and other OB-fold proteins: AlphaFold predicted structures of A3, the predicted product from *Tb927.10.8220*, MPSS5, and MPSS6 showing the higher- (blue) and lower- (orange) -confidence (pLDDT < 70) structures. OB-folds and the ZFs are noted.

CCs that perform U-insertion and deletion editing. Multiple single amino acid (saa)-LOF mutations were identified in the two ZFs, carboxy-terminal OB-fold, adjacent region domains and in a nearby IDR. Saa-LOF mutations that disrupt CC integrity show that A3 is critical to CC structure (Figs. 2–5), and previous structural studies indicate that its interaction with A6 may be especially important for this (Fig. 7A; Park and Hol 2012; Park et al. 2012b). These results complement our previous results of A3 cross-linking to seven other CC proteins (summarized in Fig. 7; Supplemental Fig. S5; Supplemental Table S6; McDermott et al. 2016). The characteristics of the OB-fold and the results of mutations which alter but do not eliminate editing suggest interactions between A3 and substrate RNA. These may normally be associated with the accuracy and/or efficiency of editing, perhaps by affecting one or more of its many steps. The greater effects of A3 mutations on CC structure and editing in BFs than PFs mirror other studies which show that CCs are inherently different between life-cycle stages despite containing the same inventory of proteins (Carnes et al. 2011, 2022; McDermott et al. 2015b). Our identification of structural homologs of A3 (Fig. 6; Supplemental Fig. S4; Supplemental Tables S4, S5) may help illuminate the roles of these proteins that have functions associated with RNA.

Multiple domains of A3 are critical for the structure and functions of the three different CCs

Each domain of A3 contributes to its overall function as is evident from the diverse effects of the mutations which range from the alteration but not loss of editing to the complete loss of CCs, their proteins and editing (summarized in Fig. 7). The C2H2 ZFs contribute to CC structural organization via their interactions with other CC proteins as shown by the effects of their mutation on CC integrity, that is, less than ~1 MDa CC material and reduced amounts of A1 protein (Fig. 2), and the cross-linking of the ZFs with A2 and B5 (Schnaufer et al. 2010; McDermott et al. 2016). The greater effect of mutations of the NTZF than the CTZF on CC structure suggests that this ZF and its adjacent fold participate in the protein interactions perhaps including proteins other than those found by cross-linking. That mutations of the ZFs alter but do not eliminate editing (Fig. 4) implies that they may also interact with RNA, perhaps transiently. The greatest impacts of ZF mutations that result from substitutions of the four C residues that coordinate the Zn^{2+} in both ZFs (Fig. 4) indicates that the A3 ZFs contribute to the network of functional protein and perhaps RNA interactions within CCs.

The A3 OB-fold contributes to CC structure and function via a variety of interactions with other CC proteins. The mutational analyses complement our previous cross-linking results which showed that the A3 OB-fold interacts with N1 and N2 in CC1 and CC2, respectively, and with A1, A6, and B5 that are in all CCs (Fig. 7; Supplemental Fig. S5; Supplemental Table S6; McDermott et al. 2016). They extend understanding of the OB-fold interactions with A1 and A6 as V311F and P379T mutations resulted in loss of A1, and likely T2 and L2, other parts of the heterotrimeric insertion subcomplex (Schnaufer et al. 2003), and reduced CC abundance. The V311 residue that is present in most of the nine analyzed editing OB-fold proteins (Supplemental Fig. S4; Supplemental Table S5; Park and Hol 2012) contributes to a proposed hydrophobic pocket on the surface of A3 (Park and Hol 2012) which may have been disrupted by the substitution to a bulky Phe suggesting that it participates in protein–protein interactions (Fig. 3). Most substitutions in or near β1 strand of the OB-fold (residues 282–305), part of which maps to the structural interface with A6 (Fig. 7; Park and Hol 2012; Park et al. 2012b), result in the absence of all CCs and their proteins (Figs. 2, 3) indicating that the interaction between the A3 OB-fold and A6 is critical for CC structure. Thus, our results and those of others (Schnaufer et al. 2010; Park and Hol 2012; Park et al. 2012b; McDermott et al. 2016) indicate that the OB-fold contributes to a network of protein–protein interactions within the CCs.

A3 contains three predicted IDR regions (Park and Hol 2012), but only the L270R mutation which is near an IDR was obtained in our random mutagenesis screen (Figs. 1, 7). This may be because the mutagenesis was not extensive or due to the practical limitation on the number of cell lines characterized. The substantial impact of the L270R mutation on editing without an overall impact on CC structure suggests that it may have affected protein or RNA interactions and/or conformations within the CCs which are critical for editing. This implies that the other IDRs in A3 also have important functions in editing,

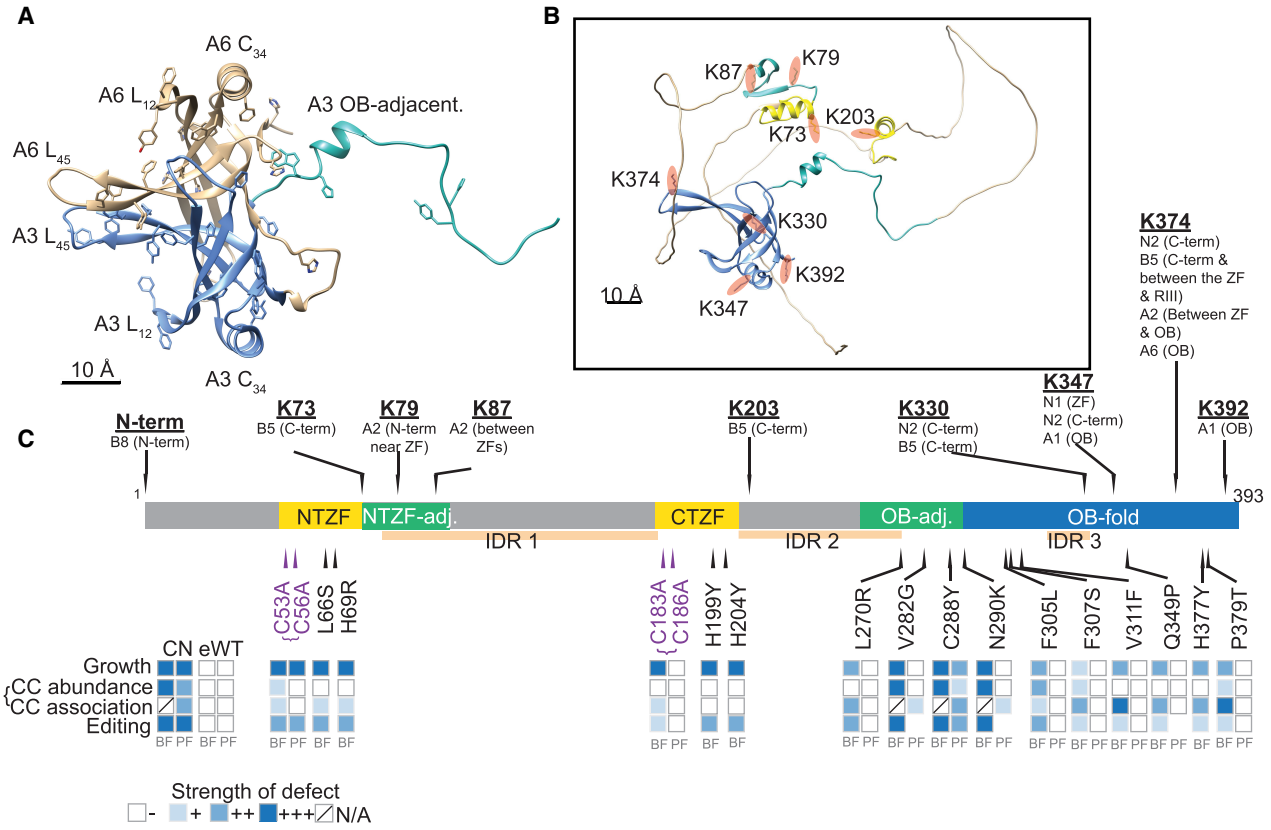

FIGURE 7. Summary of A3 protein characteristics, interactions, and effects of mutations. (*A*) Location of OB-fold domains and residues with planar side chains of the A3 OB-fold (blue) in complex with A6 (tan). (*B*) Location of cross-linked Lys residues (orange) in the predicted AlphaFold model of A3 (McDermott et al. 2016) showing the OB-fold (blue), ZFs (yellow) and ZF, and OB-fold adjacent regions (teal). (*C*) Summary diagram showing cross-links of A3 Lys residues with other CC proteins, domain locations, and effects of the mutations on cell line growth, CCs, and editing. Heat map indicates increasing strength of observed defects in CC abundance, association, and editing of A6, RPS12, and MURF2, as increasing intensity of blue shades (see legend).

perhaps by interacting with proteins or with RNA as suggested by the characteristics of these protein sequences which have been shown in other proteins to facilitate interactions with RNA (Zaharias et al. 2021; Zeke et al. 2022; Luo et al. 2023). The IDRs may provide the CCs with flexibility to accommodate many diverse substrate sequences and conformational changes during editing, like what has been shown for flexible regions in mammalian LIN28A (Nam et al. 2011; Wang et al. 2017).

RNA interactions and effects on editing

Previous results have shown that recombinant A3 can bind RNA (Brecht et al. 2005; Voigt et al. 2018) as can the OB-folds of A1–6 (Voigt et al. 2018). The characteristics of the A3 OB-fold have structural similarities to the OB-folds of other proteins that bind RNA or DNA via a combination of base stacking and electrostatic interactions involving planar and charged amino acids (Theobald et al. 2003; Horvath 2011; Wang et al. 2017). Notably, previous mutational analysis of the related OB-fold of A1 showed that the basic charges of three Arg residues facilitate interactions between A1 and RNA in vitro (Park et al. 2012a). A3 has conserved Arg residues (R336 and R363) at two of these three positions that could also interact with RNA (Supplemental Fig. S4A). The location of these residues near the groove formed by L_{12} and L_{45}, which contains many planar residues including F305, F307, and H377, suggests that the OB-fold of A3 binds RNA via both planar and charged interactions.

That several A3 OB-fold mutations caused lesser effects on CC structure but resulted in anomalous editing (Figs. 1–5) suggests that some of these mutations might have affected interactions between A3 and RNA. Given the interaction between A3 and A6, two or more OB-folds may cooperatively bind RNA, possibly via a mechanism analogous to SSB tetramer binding ssDNA (Antony et al. 2012). The available information does not indicate which strand of RNA may interact with each OB-fold, but an attractive possibility is that one binds mRNA while another binds gRNA. Alternatively, the OB-folds might work together to resolve secondary structures in the mRNA as has been previously suggested (Voigt et al. 2018). The editing substrate may also interact with other domains of A3 including its ZFs and IDRs, both of which have been

implicated in RNA binding in other systems (Tompa and Csermely 2004; Dyson 2012; Corley et al. 2020; Zaharias et al. 2021; Luo et al. 2023).

Developmental differences in editing

Differences in phenotypes resulting from the same substitutions in BF versus PF indicate that A3 functions differently between the life-cycle stages (Figs. 3–6). There are several nonmutually exclusive possibilities that may explain the different BF versus PF phenotypes: (i) A3 may undergo PTMs that are life-cycle stage specific, (ii) A3 may interact with accessory factors that are present or function in editing in specific life-cycle stages, and (iii) there may be conformational differences in BF versus PF CCs, that result in different A3 interactions with other CC proteins in BF versus PF. Any of these possibilities may also be influenced by factors such as temperature, which differs between the life-cycle stages and may impact RNA modification pathways (McDermott et al. 2015b; Chikne et al. 2016; Rajan et al. 2019). The results reported here mirror our previous results that show that CCs appear physically and functionally different between life-cycle stages despite having the same set of proteins (Carnes et al. 2011, 2022; Guo et al. 2012; McDermott et al. 2015a,b; McDermott and Stuart 2017). The stabilities of CCs and CC proteins are more sensitive in BF relative to PF to most mutations or loss of CC proteins and most mutations of B5–B8 have greater effects on CC stability in BFs than PFs (Fig. 2; Carnes et al. 2011, 2022; Guo et al. 2012; McDermott et al. 2015a,b; McDermott and Stuart 2017). This implies that domain interactions may have lower affinities in BFs than PFs. Nevertheless, some mutations of CC proteins have the reciprocal life-cycle stage specific effects, that is, detrimental in PF but not BF. These include the H233A mutation in the RAM motif of B5 that resulted in disruption of CCs and editing, and multiple mutations identified by deep mutational scanning of the RNase III domain of B4 (SM McDermott and KD Stuart, unpubl.). The mechanisms underlying the differential editing are unknown (Schnaufer et al. 2002; McDermott et al. 2015b), but they likely involve interactions within CCs and between CCs, SCs and accessory factors (Aphasizheva et al. 2020; Carnes et al. 2023) that impact substrate specificities and kinetic characteristics of the multiple editing steps.

The proximity of A3 to other proteins within the CCs (McDermott et al. 2016) and the impact of mutations to A3 on CC integrity and RNA editing suggests that A3 functions in the structural organization and intramolecular positioning of proteins and substrate RNA within the three different CCs during editing. A3 may interact differently in CC1, CC2, and CC3 and affect ES binding and cleavage by their different endonucleases which initiates the editing of each ES and differentially affect the post-cleavage steps in editing. The impacts of single amino acid substitutions near the A3 interface with A6 (V282G, C288Y, and N290K) on CC integrity and editing show that this region is critical to CC stability (Fig. 7A; Wu et al. 2011; Park and Hol 2012; Park et al. 2012b). Mutations of A3 might affect its interactions with RNA and other complexes, but further detailed analyses will be necessary to elucidate the specific effects of these mutations on each of the three distinct CCs and on other components of the editing machinery, for example, SCs. The structural homology between A3 and other proteins involved with mt RNA processing for example, MPsome proteins (Fig. 6; Supplemental Fig. S4; Supplemental Tables S4, S5) suggests that they have some similar functional characteristics which may aid elucidating their specific functions. Variants of the ZF, IDR, and OB-fold domains of A3 function in a wide range of critical processes that entail protein and nucleic acid interactions which span DNA replication, repair and telomere maintenance as well as transcription, tRNA and microRNA processing, translation, and others (Allison et al. 1998; Brevet et al. 2003; Theobald et al. 2003; Horvath 2011; Nam et al. 2011; Kapps et al. 2016; Wang et al. 2017; Amir et al. 2018; Gao et al. 2018). Results from this study may contribute the understanding of the roles of these domains in RNA editing and other processes.

MATERIALS AND METHODS

Preparation of pHD1344tub(PAC)-Nterm3V5-A3 and library construction

The A3 coding sequence minus the 20-codon predicted MTS (MitoFates) (Fukasawa et al. 2015) was amplified from the pHD1344-A3-myc plasmid (Guo et al. 2010) using primers that added AttB sites (Supplemental Table S2). The resulting PCR product was first transferred into pDONR-221 via a BP clonase II reaction and then via an LR clonase II reaction into pHD1344tub(PAC)-Nterm3V5, which provides an exogenous dihydrolipoyl dehydrogenase LipDH MTS (Carnes et al. 2018). BF and PF A3 CN cells were transfected with pHD1344tub(PAC)-Nterm3V5-A3 and grown without tet to confirm expression and functional support of growth (Fig. 1). A mutagenized A3 library was produced and screened as previously described (Gray et al. 2007; McDermott et al. 2015a). Briefly, the A3 sequence specifying amino acids 21–393 was amplified from pHD1344tub(PAC)-Nterm3V5-A3 by error prone PCR, using the GeneMorphII Random Mutagenesis kit (Agilent, Cat #200523) and primers that add AttB sites (Supplemental Table S2) from 1.4 µg of plasmid which had been determined to provide an optimal mutation rate. The mutated library was cloned into the pENTR-Express donor vector via a Gateway BP Clonase II reaction (Thermo Fisher), transformed into *Escherichia coli* and plated on LB-agar containing 1 mM IPTG and 40 µg/mL kanamycin to eliminate frameshift and truncation mutants. The A3 stop codon that would interfere with the Kanamycin screening was eliminated during PCR amplification prior to library preparation.

The equivalent of ~10,000 Kanamycin-resistant clones were transferred into pHD1433tub(PAC)-Nterm3V5 via a Gateway LR Clonase II reaction resulting in the pHD1344tub(PAC)-Nterm3V5-A3 mutagenesis library. The Gateway cloning of the

mutated A3 sequence lacking a stop codon into pHD1344tub (PAC)-Nterm3V5-A3 resulted in an additional nine amino acids at the carboxyl terminus of A3 that are absent in exclusively expressed WT A3 used in the A3 CN eWT cell line. The nine residues are present in the *eWT* allele used in the A3 CN + MGA eWT cell line. To assess the nature of the mutated A3 cloned library, 48 library clones were sequenced with primers 9571 and 11,512, from which we estimate that 48.9% of the clones in the library have one or two amino acid changes, 25.5% have three or more changes, and the remaining 25.6% have no changes.

Library screening

The mutated library was screened as previously described (McDermott et al. 2015a). The pHD1344tub(PAC)-Nterm3V5-A3 library was linearized with Not1, transfected into 1.5×10^8 BF A3 CN cells (Guo et al. 2008), selected with 0.1 µg/mL puromycin, and the cells were maintained in HMI-9 with penicillin–streptomycin, 10% FBS, and 5 ng/mL tetracycline, which is the minimum amount that allows normal cell growth. Cells were plated in 24-well plates at a density of approximately one transfected cell per well, which resulted in 634 puromycin-resistant cell lines. These potential cell clones were consolidated into seven 96-well plates, replica plated at a 1:100 dilution into media plus or minus tetracycline. The cells were grown for 3 d, then passaged into another set of 96-well plates with plus or minus tet media for another 3 d. Following a total of 6 d of growth ±tet, 20 µL of alamarBlue Cell Viability Reagent (Thermo Fisher) was added to each well and the plates were incubated for 4 h. Fluorescence was measured using a SpectraMax M2 microplate reader (Molecular Devices) with an excitation wavelength of 544 nm and an emission wavelength of 590 nm to identify wells with viable (pink) and nonviable cells (blue). Plates were also photographed at 24 h and checked by eye for color change. Wells that were dark blue in the −tet plate but pink in the +tet plate were considered to have a strong growth defect, whereas those that were purple had a lesser growth defect or contained some viable cells (McDermott et al. 2015a). Comparison of the tet plus and minus replica plates was used to identify 117 cell lines with a strong growth defect (blue in minus tetracycline) and 19 with a lesser growth defect (purple in minus tetracycline). These clones were consolidated into new 96-well plates, and 10 µL of confluent cells were lysed for gDNA extraction as previously described (McDermott et al. 2015a).

PCR and sequencing of mutants

A total of 59 out of the 117 full growth defect clones were sequenced using primers 9571 and 5356 or 10,150 (Supplemental Tables S1, S2). Forward and reverse sequence pairs were assembled using Geneious and aligned to the wild-type *T. brucei* 427 Lister A3 sequence to allow for identification of mutations and resulting amino acid substitutions (Supplemental Table S1). No samples with a partial (purple) growth defect were sequenced.

Reconstruction of mutations and generation of exclusive expression cell lines

Mutations of interest, either single substitutions that disrupted function, substitutions found in more than one cell line, or substitutions at residues mentioned in the literature, were reconstructed in new cell lines as single amino acid substitutions using site-directed mutagenesis (Supplemental Table S1). For positions where more than one type of amino acid substitution was identified (i.e., mutations encoding different substitutions at the same position were found in multiple clones), only one type of amino acid substitution was reconstructed in new cell lines. Reconstructed substitutions were selected to provide coverage throughout the length of A3. The pHD1344tub(PAC)-Nterm3V5-A3 plasmid was mutagenized using the QuikChange Lightning Site-Directed Mutagenesis kit (Agilent, product #210518) and primers listed in Supplemental Table S2. All mutations were confirmed by Sanger sequencing using primers 9571 and 5356 or 10,150 (Supplemental Table S2). Substitutions of the C residues in both ZF domains were made using site-directed mutagenesis and the primers listed in Supplemental Table S2. The NTZF contains both C53A and C56A substitutions, while the CTZF contains C183A and C186A, and the NTZF&CTZF plasmid contains all four C → A, mutations as previously described (Guo et al. 2008, 2010). Our new V5-tagged ZF constructs were used for our study as no protein could be detected from a previous construct, NTZF-myc, as previously described (Supplemental Fig. S6; Guo et al. 2010). Plasmids were linearized using Not1 and transfected into the BF A3 CN cell line and selected with 0.1 µg/mL puromycin, as previously described (Guo et al. 2008; Merritt and Stuart 2013). The resulting puromycin-resistant cell lines were screened using PCR with primers 5355 and 10,150 to verify integration of the plasmid into the *tubulin* locus, and western blot to check for expression of V5-tagged A3. Plasmids encoding mutations resulting in BF growth defects were also transfected into PF A3 CN cells as previously described, except for H377Y and mutations in the ZFs (Guo et al. 2008, 2010; McDermott et al. 2015b). PF transfectants were genotyped with PCR as above using primers 5355 and 10,150, and cell lysates and expression of the V5-tagged A3 were confirmed by western blot (data not shown).

Generation of A3 mutants in the BF A3 CN + MGA cell line background

The BF A3 CN + MGA cell line was made by transfecting the A3 CN cells (Guo et al. 2008) with pEnT6 + ATPaseGammaWT + 3UTR that carries the L262P mutation in gamma ATPase, and selected with blasticidin (Dean et al. 2013; Carnes et al. 2017). The resulting cell line, A3 CN + MGA, was genotyped by PCR and sequenced using primers 9530 and 9531 (Supplemental Table S2) to confirm the presence of the MGA mutation, and rescue of the A3 CN growth defect in the absence of tetracycline was confirmed. The same pHD1344tub(PAC)-Nterm3V5-A3 plasmids were transfected into the A3 CN + MGA cell line, as previously described (Guo et al. 2010; Merritt and Stuart 2013).

Cell culture and transfections

BF cells were grown in HMI-9 with 10% FBS at 37°C, 5% CO_2. PF cells were grown in SDM-79 with 10% FBS at 27°C. The PF A3 CN cell line used contained an untagged tet-regulated A3 construct expressed from the *rDNA* locus and was produced as previously described (McDermott et al. 2015b). Unless otherwise stated,

the concentrations of drugs used for selection and tet-regulated expression of transgenes in this study were as follows: for BFs, 2.5 µg/mL G418, 5 µg/mL hygromycin, 2.5 µg/mL phleomycin, 0.5 µg/mL Tet, and 0.1 µg/mL puromycin; for PFs, 15 µg/mL G418, 25 µg/mL hygromycin, 2.5 µg/mL phleomycin, 0.5 µg/mL Tet, 1 µg/mL puromycin, and 10 µg/mL blasticidin. For BF transfections, cells were washed in PBS plus 6 mM glucose, resuspended in 0.2 M sodium phosphate, 2 M KCl, 0.1 M $CaCl_2$, and 2 M HEPES, and transfected using the Amaxa Nucleofector (Lonza) program X-001 as previously described (Merritt and Stuart 2013). For PF transfections, cells were washed and resuspended in 0.5mL cytomix buffer (25 mM HEPES pH 7.6, 120 mM KCl, 0.15 mM $CaCl_2$, 10 mM K_2HPO_4/KH_2PO_4 pH 7.6, 2 mM EDTA, 6 mM glucose, 5 mM $MgCl_2$). Washed cells were then transfected using a BTX nucleofector at 1600 V, 25 Ω, 16 µF, and plated as previously described (Merritt and Stuart 2013).

Growth rate analyses

BF cells were seeded at an initial density of 2×10^5 cells/mL and PF cells at 2×10^6 cells/mL, unless noted otherwise. Cells were counted using a Z1 Coulter Particle Counter each day. BFs were reseeded at 2×10^5 cells/mL in 10 mL every day, while PF were reseeded at 2×10^6 cells/mL in 10 mL every 2 d. The ratio of cumulative cell numbers in −tet to +tet cultures for each cell line was calculated (Carnes et al. 2022). Log_2 of the ratio is displayed on a blue-orange heat map created using Microsoft Excel. Growth rate analyses in Figure 1 are from one biological replicate. One clone from each cell line was used for this and other experiments.

Glycerol gradient fractionation

Glycerol gradients were run as previously described (McDermott et al. 2015a). Briefly, 3×10^9 BFs were grown in the absence of tet for 72 h, collected by centrifugation and washed with PBS plus 6 mM glucose. Cell pellets were flash frozen in liquid nitrogen and stored at −80°C until use. Pellets were lysed in 500–1000 µL of lysis buffer containing 10 mM Tris pH 7.2, 10 mM $MgCl_2$, and 100 mM KCl supplemented with cOmplete Mini Protease-Inhibitor Tablets (Roche), pepstatin A, leupeptin, Pefabloc (Roche), and 1 mM DTT. Triton-X100 was then added to a final concentration of 1%. Cells were incubated on ice for 10 min followed by centrifugation at 13,000 rpm in a microcentrifuge to clear. An amount of 50–100 µL of the cleared lysate was taken for a western blot and the remainder was loaded onto 11 mL 10%–30% glycerol gradients and centrifuged in a Beckman Optima XPN-80 Ultracentrifuge for 9 h at 38,000 rpm using an SW40 rotor. A total of 500 µL fractions were collected from the top and 100 µL samples were taken for analysis by both native and SDS-PAGE western blots. The remaining fractions were flash frozen in liquid nitrogen and stored at −80°C. Western blots from gradients were developed using either ECL (Pierce) or SuperSignal West PICO Plus ECL (Pierce) and imaged using X-ray film (McKesson).

SDS-PAGE, BN-PAGE, and western blotting

Western blots were conducted as previously described (Carnes et al. 2022). Briefly, cell pellets containing 5×10^7–2×10^8 cells were resuspended on ice in IPP150 buffer (10 mM Tris-HCL pH 8.0, 150 mM NaCl, and 0.1% NP-40) with cOmplete Protease-Inhibitor Cocktail Mini Tablets (Roche). Triton-X100 was added to a final concentration of 1% and the samples were incubated on ice for 10–20 min to lyse the cells. Lysates were cleared by centrifugation at 13,000 rpm in a microcentrifuge for 10 min, diluted 1:1 in Tricine sample buffer (Bio-Rad) with β-mercaptoethanol, and up to ∼6×10^6 cell equivalents were loaded onto each lane of 10% TGX-acrylamide Criterion gels (Bio-Rad). Gels were run at 100V for ∼2 h or until the dye front ran off the gel. Protein was transferred to a PVDF Membrane (Millipore) using a Tris/glycine transfer buffer with 20% methanol. Membranes were blocked in PBS-Tween with 5% milk for 15 min before the addition of primary antibody. Antibodies and dilutions are listed in Supplemental Table S7. Western blots were exposed to ECL (Pierce) and visualized using X-ray film (McKesson). For BN-PAGE, cleared lysates were prepared the same as for the denaturing western blots. A total of 5×10^6 cell equivalents were loaded into wells on a 3%–12% Bis-Tris gradient gel with unstained NativePage protein standards in the first well (Thermo Fisher) and run according to manufacturer's instructions. Protein was then transferred to a PVDF Membrane (Millipore) overnight with NuPAGE Transfer Buffer (Thermo Fisher) without methanol at 22–24 V at 4°C. Following transfer, gels were stained with Ponceau SP to visualize the protein standards, fixed in 10% acetic acid, and probed with antibodies (Supplemental Table S7). All western blots were imaged using X-ray film (McKesson) and are thus semiquantitative. Western blots shown in Figure 2 are representative of at least two biological replicates.

RNA extraction, RT-PCR, and qPCR

All procedures for RNA extraction, quantification, cDNA synthesis, and qPCR were designed to follow the MIQE guidelines. Briefly, 1×10^8 cells were harvested by centrifugation, washed with PBS and 6 mM glucose, resuspended in TRIzol, and stored at −80°C until use. Total RNA was extracted from the TRIzol samples; quality was checked using a BioAnalyzer (Agilent) and quantified using the NanoDrop One Spectrophotometer (Thermo Fisher). RNAs were treated with DNase I, and cDNA was generated using random hexamer primers with TaqMan Reverse Transcription Reagents and MultiScribe Reverse Transcriptase (Thermo Fisher). Prior to qPCR, cDNAs were preamplified using Taqman PreAmp Master Mix (Thermo Fisher), treated with Exonuclease I to remove excess primers, and diluted as previously described (McDermott et al. 2015a). High-throughput BioMark qPCR was performed as previously described using SsoFast EvaGreen with low ROX (Bio-Rad) and the Fluidigm BioMark HD system (McDermott et al. 2015b). Data were analyzed using the Fluidigm Real-Time PCR Analysis software and Microsoft Excel. In most cases, heat maps were generated using the average of two or three biological replicates with two technical replicates each. However, there is only one ND7 3′ ed and ND8 ed biological replicate for V311F, H377Y, and P379T. Primers used for this assay are listed in Supplemental Table S2. For RT-PCR (Fig. 4), cDNA was synthesized from 1 µg of RNA using MultiScribe Reverse Transcriptase (Invitrogen) and a gene-specific reverse primer (4394 [MURF2], 5380 [A6], 3620 [RPS12], or 3707 [ND4]) (Supplemental Table S2). The entire amount of cDNA was

used in a PCR reaction to amplify MURF2, RPS12, A6, or ND4 transcripts using primer pairs 6204/4934 (MURF2), 3704/3580 (A6), 3619/3620 (RPS12), and 3706/3707 (ND4) (Supplemental Table S2; Carnes et al. 2022). PCR products were resolved on a 3% agarose gel containing ethidium bromide and visualized. RT-PCR products shown in Figure 4 are representative of at least two biological replicates for the CN-background cell lines and one replicate for the MGA background cell lines.

Cloning and Sanger sequencing of RT-PCR products

The remaining RT-PCR products from Figure 4 were resolved on an 1.5% agarose gel, and all RPS12 products spanning pre-edited through edited sizes (~200–350 bp) were excised for each sample (BF L270R, BF eWT, and BF CN), purified, and cloned into pGEM-T-Easy (Promega), according to manufacturer's instructions. Ligations were transformed into 5α *E. coli* (NEB) and plated on Amp/IPTG/X-gal plates for blue/white screening. White colonies were selected for Sanger sequenced using T7 and M13R primers and assembled using Geneious. Eleven clones for eWT, 24 clones for L270R, 13 clones for F307S, and 16 clones for P379T were analyzed. Four clones from the CN were also obtained. Editing events were determined and sequences aligned by hand. Editing sites were defined as each position between two non-U nucleotides, beginning with the most 3′ deletion site in RPS12, as this region was not spanned by primer 3620 used for RT-PCR. Editing at each site was then tabulated for each set of samples and recorded as follows: I-Ed. = expected insertion sites that are edited (the number of Us matches the fully edited [F.E.] RPS12 sequence), I-Part. Ed. = partially edited insertion sites (do not match F.E. or Pre-edited [P.E.] RPS12), D-Ed. = edited deletion sites, D-Part. Ed. = partially edited deletion sites, N-Part. Ed. = partial editing at a site that is nonedited in F.E. RPS12, not edited, and N/A = a clone contained an A, C, or G mismatch so it could not be analyzed at one or more ESs. Graphs, which show the type of editing at each site as a percent of total transcripts, were generated using Microsoft Excel. Graphs include all potential ESs (positions between non-U nucleotides). The type of editing (insertion, deletion, or no editing) expected at each site based on the fully edited RPS12 sequence is indicated beneath each bar by a yellow (insertion), blue (deletion), or black (no editing) dot. The approximate locations of the most abundant gRNAs (Kirby et al. 2016) are shown. Aligned sequences from each set of samples are shown in Supplemental Figure S3. Statistical analysis: The total number of sites with any editing (i.e., do not match a pre-edited sequence), were counted for each clone from each set of samples excluding clones with non-U mismatches. The *T*-tests shown in Supplemental Table S3 determined in Excel compare the mean number of edited sites for each mutant compared to eWT. The raw data showing the number of edited sites per clone are in Supplemental Table S3.

Protein structure modeling

The predicted structure of the *T. brucei* A3, MPSS5, MPSS6, and the protein product encoded by *Tb927.10.8220* (Uniprot IDs D6XMN0, Q38F66, Q584T7, and Q38AE2, respectively) shown in Figures 1, 6 as well as the cross-linking partners of A3 and the other OB-fold proteins shown in Supplemental Figures S4, S5 (N1 = Q4GZ50, N2 = Q38B60, B8 = Q57X13, A1 = Q586L9, A2 = Q38AE3, B5 = Q387F6, A4 = Q83B91, A5 = Q57YG2), were obtained from the AlphaFold Protein Structure Database version 2022-11-01, created with the AlphaFold Monomer v2.0 pipeline (https://alphafold.ebi.ac.uk/) (Jumper et al. 2021; Varadi et al. 2022). A Dali structural homology search was conducted using A3 (D6XMN0) (http://ekhidna2.biocenter.helsinki.fi/dali/) (Holm 2022). Only proteins that may localize to the mitochondrion are listed in Supplemental Table S4. Potential cognate residues in proteins with structural similarity to A3 (Supplemental Table S5; Supplemental Fig. S4) were visually identified using the AlphaFold structures of each protein in comparison to A3. The structural overlays shown in Supplemental Figure S4 were produced using the matchmaker function in Chimera and residues that are comparable to those mutated in A3 are indicated.

Multiple sequence alignments

Sequence alignments in Figure 1 and Supplemental Figure S1 were constructed using the MUSCLE alignment tool in Geneious. The alignment was highlighted using the Blosum 62 matrix, threshold 1 in Geneious. The gene IDs for *T. brucei*, *T. cruzi*, and *T. congolense* A3 used for the alignment are Tb427.08.620, TcCLB.509611.110, and TcIL3000_8_100.1, respectively.

SUPPLEMENTAL MATERIAL

Supplemental material is available for this article.

ACKNOWLEDGMENTS

This work was supported by National Institutes of Health grant R01AI014102 to K.D.S. We thank Xuemin Guo for providing the A3 CN cell lines.

Received April 19, 2023; accepted June 30, 2023.

REFERENCES

Allison TJ, Wood TC, Briercheck DM, Rastinejad F, Richardson JP, Rule GS. 1998. Crystal structure of the RNA-binding domain from transcription termination factor rho. *Nat Struct Biol* **5:** 352–356. doi:10.1038/nsb0598-352

Amir M, Kumar V, Dohare R, Islam A, Ahmad F, Hassan MI. 2018. Sequence, structure and evolutionary analysis of cold shock domain proteins, a member of OB fold family. *J Evol Biol* **31:** 1903–1917. doi:10.1111/jeb.13382

Antony E, Weiland EA, Korolev S, Lohman TM. 2012. *Plasmodium falciparum* SSB tetramer wraps single-stranded DNA with similar topology but opposite polarity to *E. coli* SSB. *J Mol Biol* **420:** 269–283. doi:10.1016/j.jmb.2012.04.021

Aphasizheva I, Aphasizhev R. 2016. U-insertion/deletion mRNA-editing holoenzyme: definition in sight. *Trends Parasitol* **32:** 144–156. doi:10.1016/j.pt.2015.10.004

Aphasizheva I, Zhang L, Wang X, Kaake RM, Huang L, Monti S, Aphasizhev R. 2014. RNA binding and core complexes constitute the U-insertion/deletion editosome. *Mol Cell Biol* **34:** 4329–4342. doi:10.1128/MCB.01075-14

Aphasizheva I, Alfonzo J, Carnes J, Cestari I, Cruz-Reyes J, Göringer HU, Hajduk S, Lukeš J, Madison-Antenucci S,

Maslov DA, et al. 2020. Lexis and grammar of mitochondrial RNA processing in trypanosomes. *Trends Parasitol* **36:** 337–355. doi:10.1016/j.pt.2020.01.006

Benne R, Van den Burg J, Brakenhoff JP, Sloof P, Van Boom JH, Tromp MC. 1986. Major transcript of the frameshifted *coxII* gene from trypanosome mitochondria contains four nucleotides that are not encoded in the DNA. *Cell* **46:** 819–826. doi:10.1016/0092-8674(86)90063-2

Bhat GJ, Koslowsky DJ, Feagin JE, Smiley BL, Stuart K. 1990. An extensively edited mitochondrial transcript in kinetoplastids encodes a protein homologous to ATPase subunit 6. *Cell* **61:** 885–894. doi:10.1016/0092-8674(90)90199-O

Brecht M, Niemann M, Schluter E, Muller UF, Stuart K, Goringer HU. 2005. TbMP42, a protein component of the RNA editing complex in African trypanosomes, has endo-exoribonuclease activity. *Mol Cell* **17:** 621–630. doi:10.1016/j.molcel.2005.01.018

Brevet A, Chen J, Commans S, Lazennec C, Blanquet S, Plateau P. 2003. Anticodon recognition in evolution: switching tRNA specificity of an aminoacyl-tRNA synthetase by site-directed peptide transplantation. *J Biol Chem* **278:** 30927–30935. doi:10.1074/jbc.M302618200

Carnes J, Soares CZ, Wickham C, Stuart K. 2011. Endonuclease associations with three distinct editosomes in *Trypanosoma brucei*. *J Biol Chem* **286:** 19320–19330. doi:10.1074/jbc.M111.228965

Carnes J, Lewis Ernst N, Wickham C, Panicucci B, Stuart K. 2012. KREX2 is not essential for either procyclic or bloodstream form *Trypanosoma brucei*. *PLoS One* **7:** e33405. doi:10.1371/journal.pone.0033405

Carnes J, McDermott S, Anupama A, Oliver BG, Sather DN, Stuart K. 2017. In vivo cleavage specificity of *Trypanosoma brucei* editosome endonucleases. *Nucleic Acids Res* **45:** 4667–4686. doi:10.1093/nar/gkx116

Carnes J, McDermott SM, Stuart K. 2018. RNase III domain of KREPB9 and KREPB10 association with editosomes in *Trypanosoma brucei*. *mSphere* **3:** e00585-17. doi:10.1128/mSphereDirect.00585-17

Carnes J, McDermott SM, Lewis I, Tracy M, Stuart K. 2022. Domain function and predicted structure of three heterodimeric endonuclease subunits of RNA editing catalytic complexes in *Trypanosoma brucei*. *Nucleic Acids Res* **50:** 10123–10139. doi:10.1093/nar/gkac753

Carnes J, Gendrin C, McDermott SM, Stuart K. 2023. KRGG1 function in RNA editing in *Trypanosoma brucei*. *RNA* **29:** 228–240. doi:10.1261/rna.079418.122

Chikne V, Doniger T, Rajan KS, Bartok O, Eliaz D, Cohen-Chalamish S, Tschudi C, Unger R, Hashem Y, Kadener S, et al. 2016. A pseudouridylation switch in rRNA is implicated in ribosome function during the life cycle of *Trypanosoma brucei*. *Sci Rep* **6:** 25296. doi:10.1038/srep25296

Corley M, Burns MC, Yeo GW. 2020. How RNA-binding proteins interact with RNA: molecules and mechanisms. *Mol Cell* **78:** 9–29. doi:10.1016/j.molcel.2020.03.011

Dean S, Gould MK, Dewar CE, Schnaufer AC. 2013. Single point mutations in ATP synthase compensate for mitochondrial genome loss in trypanosomes. *Proc Natl Acad Sci* **110:** 14741–14746. doi:10.1073/pnas.1305404110

Deng J, Ernst NL, Turley S, Stuart KD, Hol WG. 2005. Structural basis for UTP specificity of RNA editing TUTases from *Trypanosoma brucei*. *EMBO J* **24:** 4007–4017. doi:10.1038/sj.emboj.7600861

Dubey AP, Tylec BL, McAdams NM, Sortino K, Read LK. 2021. Trypanosome RNAEditing substrate binding complex integrity and function depends on the upstream action of RESC10. *Nucleic Acids Res* **49:** 3557–3572. doi:10.1093/nar/gkab129

Dyson HJ. 2012. Roles of intrinsic disorder in protein-nucleic acid interactions. *Mol Biosyst* **8:** 97–104. doi:10.1039/C1MB05258F

Ernst NL, Panicucci B, Igo RP Jr, Panigrahi AK, Salavati R, Stuart K. 2003. TbMP57 is a 3′ terminal uridylyl transferase (TUTase) of the *Trypanosoma brucei* editosome. *Mol Cell* **11:** 1525–1536. doi:10.1016/S1097-2765(03)00185-0

Ernst NL, Panicucci B, Carnes J, Stuart K. 2009. Differential functions of two editosome exoUases in *Trypanosoma brucei*. *RNA* **15:** 947–957. doi:10.1261/rna.1373009

Feagin JE, Jasmer DP, Stuart K. 1987. Developmentally regulated addition of nucleotides within apocytochrome b transcripts in *Trypanosoma brucei*. *Cell* **49:** 337–345. doi:10.1016/0092-8674(87)90286-8

Feagin JE, Abraham JM, Stuart K. 1988. Extensive editing of the cytochrome c oxidase III transcript in *Trypanosoma brucei*. *Cell* **53:** 413–422. doi:10.1016/0092-8674(88)90161-4

Fukasawa Y, Tsuji J, Fu SC, Tomii K, Horton P, Imai K. 2015. MitoFates: improved prediction of mitochondrial targeting sequences and their cleavage sites. *Mol Cell Proteom* **14:** 1113–1126. doi:10.1074/mcp.M114.043083

Gao S, Feng S, Ning S, Liu J, Zhao H, Xu Y, Shang J, Li K, Li Q, Guo R, et al. 2018. An OB-fold complex controls the repair pathways for DNA double-strand breaks. *Nat Commun* **9:** 3925. doi:10.1038/s41467-018-06407-7

Gray PN, Busser KJ, Chappell TG. 2007. A novel approach for generating full-length, high coverage allele libraries for the analysis of protein interactions. *Mol Cell Proteom* **6:** 514–526. doi:10.1074/mcp.T600023-MCP200

Guo X, Ernst NL, Stuart KD. 2008. The KREPA3 zinc finger motifs and OB-fold domain are essential for RNA editing and survival of *Trypanosoma brucei*. *Mol Cell Biol* **28:** 6939–6953. doi:10.1128/MCB.01115-08

Guo X, Ernst NL, Carnes J, Stuart KD. 2010. The zinc-fingers of KREPA3 are essential for the complete editing of mitochondrial mRNAs in *Trypanosoma brucei*. *PLoS One* **5:** e8913. doi:10.1371/journal.pone.0008913

Guo X, Carnes J, Ernst NL, Winkler M, Stuart K. 2012. KREPB6, KREPB7, and KREPB8 are important for editing endonuclease function in *Trypanosoma brucei*. *RNA* **18:** 308–320. doi:10.1261/rna.029314.111

Hashimi H, Cicová Z, Novotná L, Wen YZ, Lukes J. 2009. Kinetoplastid guide RNA biogenesis is dependent on subunits of the mitochondrial RNA binding complex 1 and mitochondrial RNA polymerase. *RNA* **15:** 588–599. doi:10.1261/rna.1411809

Holm L. 2022. Dali server: structural unification of protein families. *Nucleic Acids Res* **50:** W210–W215. doi:10.1093/nar/gkac387

Horvath MP. 2011. Structural anatomy of telomere OB proteins. *Crit Rev Biochem Mol Biol* **46:** 409–435. doi:10.3109/10409238.2011.609295

Jumper J, Evans R, Pritzel A, Green T, Figurnov M, Ronneberger O, Tunyasuvunakool K, Bates R, Žídek A, Potapenko A, et al. 2021. Highly accurate protein structure prediction with AlphaFold. *Nature* **596:** 583–589. doi:10.1038/s41586-021-03819-2

Kapps D, Cela M, Theobald-Dietrich A, Hendrickson T, Frugier M. 2016. OB or not OB: idiosyncratic utilization of the tRNA-binding OB-fold domain in unicellular, pathogenic eukaryotes. *FEBS Lett* **590:** 4180–4191. doi:10.1002/1873-3468.12441

Kirby LE, Sun Y, Judah D, Nowak S, Koslowsky D. 2016. Analysis of the *Trypanosoma brucei* EATRO 164 bloodstream guide RNA transcriptome. *PLoS Negl Trop Dis* **10:** e0004793. doi:10.1371/journal.pntd.0004793

Koslowsky DJ, Bhat GJ, Perrollaz AL, Feagin JE, Stuart K. 1990. The MURF3 gene of *T. brucei* contains multiple domains of extensive editing and is homologous to a subunit of NADH dehydrogenase. *Cell* **62:** 901–911. doi:10.1016/0092-8674(90)90265-G

Koslowsky DJ, Riley GR, Feagin JE, Stuart K. 1992. Guide RNAs for transcripts with developmentally regulated RNA editing are present in both life cycle stages of *Trypanosoma brucei*. *Mol Cell Biol* **12:** 2043–2049. doi:10.1128/mcb.12.5.2043-2049.1992

Law JA, O'Hearn SF, Sollner-Webb B. 2008. *Trypanosoma brucei* RNA editing protein TbMP42 (band VI) is crucial for the endonucleolytic cleavages but not the subsequent steps of U-deletion and U-insertion. *RNA* **14:** 1187–1200. doi:10.1261/rna.899508

Luo Y, Pratihar S, Horste EH, Mitschka S, Mey ASJS, Al-Hashimi HM, Mayr C. 2023. mRNA interactions with disordered regions control protein activity. bioRxiv doi:10.1101/2023.02.18.529068

McDermott SM, Stuart K. 2017. The essential functions of KREPB4 are developmentally distinct and required for endonuclease association with editosomes. *RNA* **23:** 1672–1684. doi:10.1261/rna.062786.117

McDermott SM, Carnes J, Stuart K. 2015a. Identification by random mutagenesis of functional domains in KREPB5 that differentially affect RNA editing between life cycle stages of *Trypanosoma brucei*. *Mol Cell Biol* **35:** 3945–3961. doi:10.1128/MCB.00790-15

McDermott SM, Guo X, Carnes J, Stuart K. 2015b. Differential editosome protein function between life cycle stages of *Trypanosoma brucei*. *J Biol Chem* **290:** 24914–24931. doi:10.1074/jbc.M115.669432

McDermott SM, Luo J, Carnes J, Ranish JA, Stuart K. 2016. The architecture of *Trypanosoma brucei* editosomes. *Proc Natl Acad Sci* **113:** E6476–E6485. doi:10.1073/pnas.1610177113

McManus MT, Shimamura M, Grams J, Hajduk SL. 2001. Identification of candidate mitochondrial RNA editing ligases from *Trypanosoma brucei*. *RNA* **7:** 167–175. doi:10.1017/S1355838201002072

Merritt C, Stuart K. 2013. Identification of essential and non-essential protein kinases by a fusion PCR method for efficient production of transgenic *Trypanosoma brucei*. *Mol Biochem Parasitol* **190:** 44–49. doi:10.1016/j.molbiopara.2013.05.002

Nam Y, Chen C, Gregory RI, Chou JJ, Sliz P. 2011. Molecular basis for interaction of let-7 microRNAs with Lin28. *Cell* **147:** 1080–1091. doi:10.1016/j.cell.2011.10.020

Palazzo SS, Panigrahi AK, Igo RP, Salavati R, Stuart K. 2003. Kinetoplastid RNA editing ligases: complex association, characterization, and substrate requirements. *Mol Biochem Parasitol* **127:** 161–167. doi:10.1016/S0166-6851(02)00333-X

Panigrahi AK, Schnaufer A, Carmean N, Igo RP, Gygi SP, Ernst NL, Palazzo SS, Weston DS, Aebersold R, Salavati R, et al. 2001. Four related proteins of the *Trypanosoma brucei* RNA editing complex. *Mol Cell Biol* **21:** 6833–6840. doi:10.1128/MCB.21.20.6833-6840.2001

Panigrahi AK, Zíková A, Dalley RA, Acestor N, Ogata Y, Anupama A, Myler PJ, Stuart KD. 2008. Mitochondrial complexes in *Trypanosoma brucei*: a novel complex and a unique oxidoreductase complex. *Mol Cell Proteom* **7:** 534–545. doi:10.1074/mcp.M700430-MCP200

Park YJ, Hol WG. 2012. Explorations of linked editosome domains leading to the discovery of motifs defining conserved pockets in editosome OB-folds. *J Struct Biol* **180:** 362–373. doi:10.1016/j.jsb.2012.07.012

Park YJ, Budiarto T, Wu M, Pardon E, Steyaert J, Hol WG. 2012a. The structure of the C-terminal domain of the largest editosome interaction protein and its role in promoting RNA binding by RNA-editing ligase L2. *Nucleic Acids Res* **40:** 6966–6977. doi:10.1093/nar/gks369

Park YJ, Pardon E, Wu M, Steyaert J, Hol WG. 2012b. Crystal structure of a heterodimer of editosome interaction proteins in complex with two copies of a cross-reacting nanobody. *Nucleic Acids Res* **40:** 1828–1840. doi:10.1093/nar/gkr867

Penschow JL, Sleve DA, Ryan CM, Read LK. 2004. TbDSS-1, an essential *Trypanosoma brucei* exoribonuclease homolog that has pleiotropic effects on mitochondrial RNA metabolism. *Eukaryot Cell* **3:** 1206–1216. doi:10.1128/EC.3.5.1206-1216.2004

Pollard VW, Rohrer SP, Michelotti EF, Hancock K, Hajduk SL. 1990. Organization of minicircle genes for guide RNAs in *Trypanosoma brucei*. *Cell* **63:** 783–790. doi:10.1016/0092-8674(90)90144-4

Rajan KS, Doniger T, Cohen-Chalamish S, Chen D, Semo O, Aryal S, Glick Saar E, Chikne V, Gerber D, Unger R, et al. 2019. Pseudouridines on *Trypanosoma brucei* spliceosomal small nuclear RNAs and their implication for RNA and protein interactions. *Nucleic Acids Res* **47:** 7633–7647. doi:10.1093/nar/gkz477

Read LK, Myler PJ, Stuart K. 1992. Extensive editing of both processed and preprocessed maxicircle CR6 transcripts in *Trypanosoma brucei*. *J Biol Chem* **267:** 1123–1128. doi:10.1016/S0021-9258(18)48405-0

Read LK, Lukes J, Hashimi H. 2016. Trypanosome RNA editing: the complexity of getting U in and taking U out. *Wiley Interdiscip Rev RNA* **7:** 33–51. doi:10.1002/wrna.1313

Riley GR, Corell RA, Stuart K. 1994. Multiple guide RNAs for identical editing of *Trypanosoma brucei* apocytochrome *b* mRNA have an unusual minicircle location and are developmentally regulated. *J Biol Chem* **269:** 6101–6108. doi:10.1016/S0021-9258(17)37575-0

Riley GR, Myler PJ, Stuart K. 1995. Quantitation of RNA editing substrates, products and potential intermediates: implications for developmental regulation. *Nucleic Acids Res* **23:** 708–712. doi:10.1093/nar/23.4.708

Schnaufer A, Panigrahi AK, Panicucci B, Igo RP Jr, Wirtz E, Salavati R, Stuart K. 2001. An RNA ligase essential for RNA editing and survival of the bloodstream form of *Trypanosoma brucei*. *Science* **291:** 2159–2162. doi:10.1126/science.1058955

Schnaufer A, Domingo GJ, Stuart K. 2002. Natural and induced dyskinetoplastic trypanosomatids: how to live without mitochondrial DNA. *Int J Parasitol* **32:** 1071–1084. doi:10.1016/S0020-7519(02)00020-6

Schnaufer A, Ernst NL, Palazzo SS, O'Rear J, Salavati R, Stuart K. 2003. Separate insertion and deletion subcomplexes of the *Trypanosoma brucei* RNA editing complex. *Mol Cell* **12:** 307–319. doi:10.1016/S1097-2765(03)00286-7

Schnaufer A, Wu M, Park YJ, Nakai T, Deng J, Proff R, Hol WG, Stuart KD. 2010. A protein-protein interaction map of trypanosome ~20S editosomes. *J Biol Chem* **285:** 5282–5295. doi:10.1074/jbc.M109.059378

Stuart K, Panigrahi AK, Schnaufer A, Drozdz M, Clayton C, Salavati R. 2002. Composition of the editing complex of *Trypanosoma brucei*. *Philos Trans R Soc Lond B Biol Sci* **357:** 71–79. doi:10.1098/rstb.2001.0994

Suematsu T, Zhang L, Aphasizheva I, Monti S, Huang L, Wang Q, Costello CE, Aphasizhev R. 2016. Antisense transcripts delimit exonucleolytic activity of the mitochondrial 3′ processome to generate guide RNAs. *Mol Cell* **61:** 364–378. doi:10.1016/j.molcel.2016.01.004

Theobald DL, Mitton-Fry RM, Wuttke DS. 2003. Nucleic acid recognition by OB-fold proteins. *Annu Rev Biophys Biomol Struct* **32:** 115–133. doi:10.1146/annurev.biophys.32.110601.142506

Tompa P, Csermely P. 2004. The role of structural disorder in the function of RNA and protein chaperones. *FASEB J* **18:** 1169–1175. doi:10.1096/fj.04-1584rev

Varadi M, Anyango S, Deshpande M, Nair S, Natassia C, Yordanova G, Yuan D, Stroe O, Wood G, Laydon A, et al. 2022. AlphaFold Protein Structure Database: massively expanding the structural coverage of protein-sequence space with high-accuracy models. *Nucleic Acids Res* **50:** D439–D444. doi:10.1093/nar/gkab1061

Voigt C, Dobrychlop M, Kruse E, Czerwoniec A, Kasprzak JM, Bytner P, Campo CD, Leeder WM, Bujnicki JM, Goringer HU.

2018. The OB-fold proteins of the *Trypanosoma brucei* editosome execute RNA-chaperone activity. *Nucleic Acids Res* **46:** 10353–10367. doi:10.1093/nar/gky668

Wang L, Nam Y, Lee AK, Yu C, Roth K, Chen C, Ransey EM, Sliz P. 2017. LIN28 zinc knuckle domain is required and sufficient to induce let-7 oligouridylation. *Cell Rep* **18:** 2664–2675. doi:10.1016/j.celrep.2017.02.044

Weng J, Aphasizheva I, Etheridge RD, Huang L, Wang X, Falick AM, Aphasizhev R. 2008. Guide RNA-binding complex from mitochondria of trypanosomatids. *Mol Cell* **32:** 198–209. doi:10.1016/j.molcel.2008.08.023

Worthey EA, Schnaufer A, Mian IS, Stuart K, Salavati R. 2003. Comparative analysis of editosome proteins in trypanosomatids. *Nucleic Acids Res* **31:** 6392–6408. doi:10.1093/nar/gkg870

Wu M, Park YJ, Pardon E, Turley S, Hayhurst A, Deng J, Steyaert J, Hol WG. 2011. Structures of a key interaction protein from the *Trypanosoma brucei* editosome in complex with single domain antibodies. *J Struct Biol* **174:** 124–136. doi:10.1016/j.jsb.2010.10.007

Zaharias S, Zhang Z, Davis K, Fargason T, Cashman D, Yu T, Zhang J. 2021. Intrinsically disordered electronegative clusters improve stability and binding specificity of RNA-binding proteins. *J Biol Chem* **297:** 100945. doi:10.1016/j.jbc.2021.100945

Zeke A, Schád É, Horváth T, Abukhairan R, Szabó B, Tantos A. 2022. Deep structural insights into RNA-binding disordered protein regions. *Wiley Interdiscip Rev RNA* **13:** e1714. doi:10.1002/wrna.1714

MEET THE FIRST AUTHOR

Brittney Davidge

***Meet the First Author(s)* is an editorial feature within *RNA*, in which the first author(s) of research-based papers in each issue have the opportunity to introduce themselves and their work to readers of *RNA* and the RNA research community. Brittney Davidge is the first author of this paper, "Multiple domains of the integral KREPA3 protein are critical for the structure and precise functions of RNA editing catalytic complexes in *Trypanosoma brucei*." She obtained her PhD from the laboratory of Dr. Jeffrey Singer at Portland State University in Portland, Oregon, where she studied the role of Cul3-based ubiquitin ligase complexes in cell cycle regulation. Brittney is currently a postdoctoral research fellow in the laboratory of Dr. Ken Stuart at Seattle Children's Research Institute where she studies RNA editing in the protozoan pathogen *Trypanosoma brucei*.**

What are the major results described in your paper and how do they impact this branch of the field?

U-insertion and deletion RNA editing in *T. brucei* is catalyzed by multisubunit protein complexes. KREPA3 (A3) is a noncatalytic but essential protein found in the complexes. First, we identified single loss of function amino acid substitutions throughout A3 that impact parasite growth, RNA editing, and the protein complexes that perform RNA editing, of which A3 is a part. Notably, these mutations were located throughout A3, which consists of two zinc-finger domains, an OB-fold, and several intrinsically disordered regions. That these mutations were located throughout the protein and caused different degrees of complex disruptions and changes to RNA-editing, indicates that A3 plays a multifunctional role during editing. Second, we identified eight other editing proteins with structural homology to A3, three of which were not previously known to be related to A3. Thus, our findings might also shed some light on the roles of these other proteins.

What led you to study RNA or this aspect of RNA science?

I started studying RNA editing during my current postdoctoral position. Following graduate school, I wanted to continue studying molecular biology but I was also interested in working with a unicellular organism. I was happy to join the Stuart lab as a postdoc where I study U-insertion and deletion RNA editing in the protozoan pathogen *T. brucei*. This type of editing, which involves insertions and deletions of U nucleotides throughout the coding region of mRNAs, occurs within the mitochondrion of *T. brucei* and related protists. It often results in substantial editing, sometimes doubling the length of the edited mRNA. I continue to be fascinated by this process and enjoy learning more about it.

If you were able to give one piece of advice to your younger self, what would that be?

One piece of advice I would give my younger self would be not to underestimate the importance of good communication skills in science. I think this includes learning to read scientific literature, write about results, contribute ideas, and ask questions of peers and mentors. I had plenty of opportunities to practice these skills as a graduate student, but I wish I had practiced these more as an undergraduate.

Are there specific individuals or groups who have influenced your philosophy or approach to science?

I have always enjoyed learning about the world around me and I am grateful to my parents as they encouraged my curiosity and interest in science from a young age. Thus far in my career, my graduate and postdoctoral advisors have had the most substantial

Continued

impacts on my approach to science. Dr. Jeffrey Singer, my graduate advisor, taught me the importance of collaboration. Over the years, I have enjoyed working with other scientists and seeing firsthand how input from colleagues can lead to more impactful research. During my time as a postdoc in the lab of Dr. Ken Stuart, I have gained more independence in the lab and improved my writing skills. I appreciate that Dr. Stuart has encouraged me to become a thorough and conscientious researcher.

What are your subsequent near- or long-term career plans?

Currently, I am continuing to study RNA editing in the Stuart lab. I am planning to eventually transition into a career in science education as I really enjoy learning and assisting others with their academic journeys.